POLITECNICO DI MILANO

DIPARTIMENTO DI SCIENZE E TECNOLOGIE AEROSPAZIALI

Tesi di Laurea Magistrale in Ingegneria Aeronautica

ANALYSIS OF ERROR SOURCES IN HIGH TEMPERATURE MEASUREMENTS BY THIN THERMOCOUPLES

Relatore: Ing. GIULIO SOLERO

Tesi di Laurea di:

OCTAVIO AMARAL GARCIA

Matricola: 10960631

ANNO ACCADEMICO 2025-2026

POLITECNICO DI MILANO

DIPARTIMENTO DI SCIENZE E TECNOLOGIE AEROSPAZIALI

Tesi di Laurea Magistrale in Ingegneria Aeronautica

ANALYSIS OF ERROR SOURCES IN HIGH TEMPERATURE MEASUREMENTS BY THIN THERMOCOUPLE

Relatore: Ing. GIULIO SOLERO

Tesi di Laurea di:

OCTAVIO AMARAL GARCIA

Matricola: 10960631

ANNO ACCADEMICO 2025-2026

ACKNOWLEDGMENTS

I would like to express my gratitude to my supervisor, Eng. Giulio Solero, for the opportunity to develop this thesis, for his guidance, support, and insights throughout the academic year. His suggestions and availability were essential to the completion of this work.

I would like to thank my mother Claudia, my father Flavio, and my brother Victor for always supporting me throughout my whole life, especially during the past nine years living abroad, in the United States and in Italy. I know this journey has been challenging both for me and for my family, and I am certain that without their love and support this would not be possible. I would like to thank my grandparents, cousins, uncles, and aunts for their prayers, love, support, and for always being there for me when I needed it the most, even through a phone call.

Finally, I would like to thank all my friends for their loyalty and love. Distance never prevented me from sharing laughter, advice, and meaningful moments with those in the United States and, especially, in Brazil. I am grateful for the friends I made in Milan, who shared the same difficulties inherent to a student living abroad, and always made me feel at home and shared many happy and special moments that I will always remember.

Octavio Amaral Garcia

ABSTRACT

Accurate hot gas temperature measurements are essential for the design, performance assessment, and safe operation of combustion systems and aerospace propulsion devices. In gas turbines and jet engines, temperature directly influences combustion efficiency, material durability, cooling system requirements, and overall engine performance. However, obtaining reliable temperature measurements in high-temperature reacting flows is challenging due to the presence of multiple error sources affecting the measurement instruments.

This thesis investigates the accuracy of temperature measurements performed using a Type-B platinum-rhodium thermocouple in a premixed methane-air combustion system. The experiments were conducted on a 10-kW premixed burner representative of practical combustion applications. Temperature data were acquired through a National Instruments data-acquisition system and then analyzed to identify, quantify, and correct the main sources of measurement uncertainty.

A comprehensive uncertainty analysis was performed, considering statistical sampling effects, thermocouple calibration errors, analog-to-digital converter quantization, radiative heat losses, and sensor dynamic response limitations. Static calibration experiments were used to determine the thermocouple calibration curve, and several interpolation models were evaluated. A fourth-order polynomial regression provided the most accurate representation of the calibration data and was selected for subsequent analyses. Dynamic calibration tests showed that the thermocouple behaves approximately as a first-order system characterized by a time constant of 0.15 seconds. Fourier analysis was additionally employed to investigate the spectral content of the measured temperature fluctuations.

The results showed that statistical and quantization uncertainties represent a relatively minor contribution to the overall measurement error, whereas calibration uncertainty and radiative heat losses constitute the dominant error mechanisms. Radiative heat loss analysis further

demonstrated that the temperature indicated by the thermocouple may significantly underestimate the actual gas temperature, especially under conditions of high emissivity and low gas velocity.

The emissivity value of 0.20 was adopted for the thermocouple, while the gas velocity during the experiments was approximately 7.00 meters per second. Under these conditions, the measured mean temperature value was 1152.50 °C, the radiative losses were approximately 87.50 °C, the total measurement uncertainty was estimated to be approximately 9.69 °C, and therefore the corrected gas temperature was estimated to be 1240.00 °C with an uncertainty of 9.69 °C.

The methodology developed in this work provides techniques to evaluate and correct thermocouple measurements in high-temperature combustion environments. The proposed approach enables a more representative estimation of the true gas temperature and contributes to improving the reliability of thermal measurements used in aerospace propulsion applications.

CONTENTS

Introduction……1

Chapter 1: Hot Gas Temperature Measurement Techniques…….……3

1.1: Thermocouples……3

1.2: Resistance Temperature Detectors……..6

1.3: Thermistors…….7

1.4: Optical Pyrometers……9

1.5: Thermal Cameras……..12

1.6: Summary…….....14

Chapter 2: Combustion and Thermal Field Fundamentals……..……16

2.1: Introduction…….....16

2.2: Fundamentals of Combustion……...16

2.3: Equivalence Ratio and Flame Temperature…….....18

2.4: Structure of a Premixed Flame……19

2.5: Temperature Field in Reacting Flows…...……...….20

2.6: Temperature Fields in Combustion Systems..…….....20

2.7: Challenges in Temperature Measurement..……...22

2.8: Link to Present Work……....22

Chapter 3: Experimental Setup and Methodology……...24

3.1: Introduction……..24

3.2: Experimental Facility……...24

3.3: Premixed Burner and Combustion Chamber……...25

3.4: Fuel Supply System…….27

3.5: Temperature Measurement System……..27

3.5.1: Thermocouple……...27

3.5.2: Thermocouple Positioning System……...28

3.6: Data Acquisition System……..29

3.7: Experimental Procedure…….....29

Chapter 4: Thermocouple Error Model and Uncertainty Analysis…….31

4.1: Objective and Approach……..31

4.2: Statistical Error……31

4.3: Systematic Error……..34

4.4: Quantization Error……...37

4.5: Thermocouple Radiation Losses…….38

4.6: Thermocouple Dynamic Analysis……...42

4.7: Fourier Analysis of the Temperature Signal……44

4.8: Summary…….48

Chapter 5: Results and Discussion……49

5.1: Statistical Analysis of the Temperature Signal…….....49

5.1.1: Analysis of the 1200-Sample Dataset……..49

5.1.2: Analysis of the 9000-Sample Dataset……..50

5.1.3: Influence of Sample Size on Statistical Convergence…….52

5.2: Systematic Error Results…….53

5.2.1: Static Calibration and Linear Regression…….53

5.2.2: Comparison of Polynomial Interpolation Models……55

5.2.3: Evaluation of the Systematic Error……..56

5.3: Quantization Error Results……..57

5.3.1: Voltage Signal Analysis……57

5.3.2: Quantization Error of the ADC……58

5.3.3: Contribution to the Overall Measurement Uncertainty……60

5.4: Thermocouple Radiation Losses……60

5.4.1: Influence of Emissivity and Gas Velocity……....60

5.4.2: Implications for Temperature Measurements…….……..62

5.4.3: Selection of a Realistic Correction…….…….….63

5.5: Thermocouple Dynamic Analysis Results……..63

5.5.1: Dynamic Calibration Curve…….……....63

5.5.2: First-Order Model Validation……...64

5.5.3: Dimensionless Response Function……...65

5.5.4: Determination of the Time Constant……66

5.5.5: Discussion of the Dynamic Effects……..67

5.6: Frequency-Domain Analysis of the Temperature Signal……68

5.6.1: Experimental Conditions…….....68

5.6.2: Fourier Spectrum…….69

5.6.3: Zoomed Spectrum and Frequency Content…….70

5.6.4: Influence of Thermocouple Dynamics…….……...70

5.6.5: Discussion of the Combustion Process……71

5.7: Final Temperature Evaluation and Overall Measurement Uncertainty……..72

5.7.1: Summary of Uncertainty Sources……....72

5.7.2: Radiation Correction and Gas Temperature Estimation……..73

5.7.3: Dynamic Response Assessment……..75

5.7.4: Frequency-Domain Analysis……...75

5.7.5: Final Remarks……76

Chapter 6: Conclusions……77

Bibliography……..80

INTRODUCTION

Hot-gas temperature measurement is essential for the design and safe operation of jet engines. A mixture of compressed air and fuel undergoes a chemical reaction inside the combustion chamber, producing extremely hot and pressurized gases that expand through a turbine. The temperature of these gases at the combustor exit is a parameter of interest for engineers and pilots, as it directly affects the engine performance, efficiency, and the lifetime of various components inside the engine. Excessive gas temperatures can lead to material degradation, especially in turbine blades at the first stages, so accurate temperature monitoring is essential for granting safe operation and effective cooling system design.

Accurate measurements of gas temperature in extreme environments such as combustion chambers and first stages of high-pressure turbines are a huge challenge. A measurement instrument introduced into the system is subjected to many sources of error, which can be related to the surroundings and to the instrument itself. Even though some of the errors can be reduced and sometimes neglected through calibration, many remain inevitable and create uncertainty in the measured values.

The sources of error encountered in temperature measurements are usually classified into random, systematic or bias, dynamic, instrumentation, and installation errors. Random errors are related to fluctuations found in repeated measurements and can be studied through statistical analysis. Systematic (or bias) errors are repeatable deviations from the true value and are often associated with heat transfer effects, calibration imperfections, and instrumentation limitations. Dynamic errors are related to the response time that an instrument takes in situations such as rapid temperature variations. Instrumentation errors include quantization errors that are encountered in the process of data acquisition. Finally, errors related to installation, such as an incorrectly positioned probe or disturbances introduced into the flow by the measurement device, can also affect the accurate monitoring of the temperature.

Different measurement techniques can be adopted, including intrusive instruments such as thermocouples and resistance temperature detectors, and non-intrusive methods such as pyrometry. Each technique has its advantages and limitations depending on the application, and therefore a tradeoff analysis must be performed to select the most appropriate measurement instrument. This work provides an overview of the main techniques used for temperature measurement, emphasizing the experimental temperature measurement of a premixed methane-air flame using a Type B thermocouple, which is composed of platinum and rhodium (Pt-Rh). This type of thermocouple is used in very high temperature environments, including gas turbines and industrial furnaces, due to their high temperature capability and stability.

The objective of this thesis is to evaluate the accuracy of thermocouple temperature measurements in a premixed methane-air flame through the identification, quantification, and correction of the principal sources of measurement error. Attention is given to statistical uncertainty, calibration errors, quantization effects, radiative heat losses, and thermocouple dynamic response in order to obtain a more representative estimate of the true gas temperature. Although the experimental investigation is performed in a controlled premixed methane-air combustion system, the methodology developed in this work is intended to be applicable to practical high-temperature combustion environments. The analysis provides a framework for improving temperature measurements in aerospace propulsion systems, such as gas turbine and jet-engine combustors, where liquid hydrocarbon fuels such as kerosene are commonly used and where accurate knowledge of the thermal field is essential for performance assessment, cooling-system design, and component durability.

CHAPTER 1

HOT GAS TEMPERATURE MEASUREMENT TECHNIQUES

A variety of instruments can be employed for the measurement of burnt-gas temperatures. These instruments are generally classified into intrusive techniques, which require direct contact between the sensor and the environment under investigation, and non-intrusive (optical) techniques [1]. The selection of an appropriate temperature measurement technique for jet-engine applications can be challenging, because the temperatures downstream of combustion chambers may approach and sometimes exceed 2000 °C. Challenges related to thermal radiation, turbulent flows, and chemical reactions are also important [2]. This chapter presents an overview and comparison between the main measurement techniques considered in this work.

1.1 THERMOCOUPLES

Thermocouples are among the most widely used temperature sensors in aerospace applications [3]. They are contact-based instruments that are relatively simple to build, easy to handle due to their small sizes, and have wide operating temperature ranges. Depending on the thermocouple type, temperatures exceeding 2000 °C can be measured [4]. The use of thermocouples in combustion environments requires consideration of factors that may lead to measurement errors, such as radiative heat losses, thermal inertia, and flow disturbance [2].

Fundamental thermoelectric principles govern the operation of a thermocouple, and the Seebeck effect is the most important one. This phenomenon describes the generation of an electromotive force in a circuit composed of two different conductive materials when a temperature difference

exists between two junctions. The thermocouple produces a voltage that is dependent on the temperature, which is usually in the order of μV/K, and it depends on the materials used [5, 6].

In theory, thermocouples are described by three thermoelectric laws: the law of homogeneous materials, the law of intermediate materials, and the law of intermediate temperatures. The first one states that two or more different conductors are required in order to generate a thermoelectric voltage in a circuit. The law of intermediate materials states that the measured voltage will not be affected in a circuit that implements additional materials, if their junctions are maintained at a uniform temperature. Finally, the law of intermediate temperatures states that the total electromotive force in the circuit depends only on the temperature of the junctions. This third law is important in the working principle of thermocouples, as it allows the use of a reference junction at a known temperature, which is usually zero degrees Celsius [5, 6].

The voltage is given by the following formula [5, 6]:

$$V = \int_{T_1}^{T_2} \left[S_B(T) - S_A(T) \right] dT$$

Equation 1.1

where S_A and S_B are the Seebeck coefficients for the two metals A and B, and T_1 and T_2 are the temperatures of the two junctions. The coefficients are nonlinear and depend on the material, temperature, and molecular structure. However, the coefficients can be assumed constant over a given temperature range, so the formula can be approximated as [5, 6]:

$$V = \left(S_B - S_A \right) \left(T_2 - T_1 \right)$$

Equation 1.2

As described by the law of intermediate temperatures, one of the thermocouple junctions is exposed to a known temperature, which enables the determination of the temperature at the measurement junction. The known temperature is usually 0 °C, and the junction exposed to it is usually called cold junction or reference junction [5, 6].

Other thermoelectric effects are important for the working principle of thermocouples, such as the Thomson and Joule effects. The Thomson effect can be described as heat released or

absorbed when an electric current flows in a conductor subjected to a temperature gradient along its length, with heat being released at the points where the current flows in the same direction as the heat flow, and absorbed otherwise [5, 6]. The Joule effect is the heat dissipation produced by the circulation of current in the thermocouple, possibly increasing the temperature of the wires. A potentiometer or a high-impedance voltage measuring instrument limits the flow of current and can minimize the Joule effect [5, 6].

There are different types of thermocouples, such as K, S, R, B, T, J, and E. They have different materials, temperature ranges, sensitivities, prices, etc. [4]. The main requirements for a good thermocouple are linearity, sufficient sensibility, stability, and reproducibility of the physical-chemical properties of materials [7].

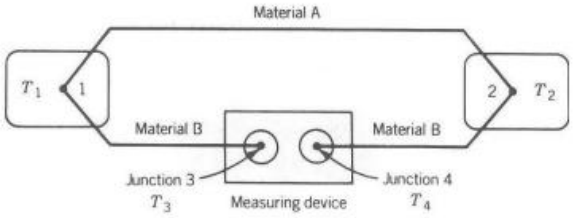

Fig 1.1: *Thermocouple circuit illustrating the Seebeck effect and the measurement and reference junctions.* [6]

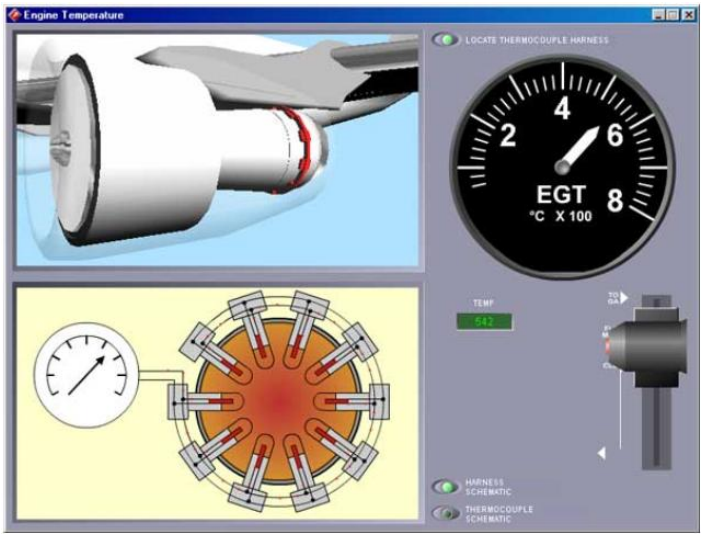

Fig 1.2: *Exhaust Gas Temperature (EGT) indication system used in aircraft engines.* [8]

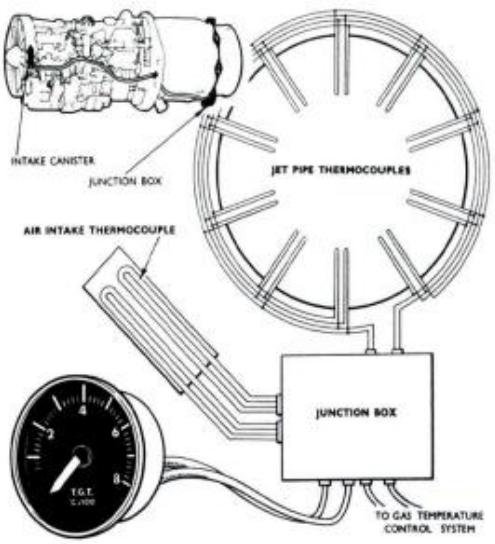

Fig 1.3: *Aircraft thermocouple-based temperature measurement system.* [9]

1.2 RESISTANCE TEMPERATURE DETECTORS

Resistance Temperature Detectors (RTD) are contact-based sensors that operate by exploiting the variation of electrical resistance with temperature. They are very accurate, stable, and used for high precision measurements. RTDs are typically constructed using metals such as platinum, copper, or nickel. Platinum is recommended as the standard thermometer by the International Temperature Scale of 1990 (ITS-90) due to its high melting point, chemical stability, resistance to oxidation, and good repeatability of the resistance-temperature characteristics [10, 11]. The resistance of a platinum resistance thermometer (PRT) can be approximated as [6, 12]:

$$R = R_0 \left[1 + \alpha(T - T_0)\right]$$

Equation 1.3

where R_0 is the value of the resistance at a temperature of 0 °C (reference temperature), and α is the linear temperature coefficient, which is equal to:

$$\alpha = \frac{R_1 - R_0}{T_1 \cdot R_0}$$

Equation 1.4

and R_1 is the resistance at a temperature equal to 100 °C. The value of α is approximately 0.0039/°C for pure Platinum [6, 11].

Despite all its advantages, RTDs are limited to lower temperature ranges, and therefore are not ideal for measuring combustion gases [13].

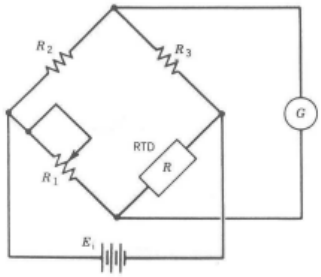

Fig 1.4: *Typical Wheatstone bridge circuit used with resistance temperature detectors.* [6]

Fig 1.5: *Industrial platinum resistance temperature detector (RTD).* [14]

1.3 THERMISTORS

Thermistors are temperature-sensitive resistors made from semiconductor materials [15]. They exhibit a strong nonlinear relationship between resistance and temperature, resulting in significantly higher sensitivity than metallic sensors such as RTDs. The relationship between temperature and resistance in a thermistor can be approximated as [15]:

$$R = R_0 \cdot e^{\beta\left(\frac{1}{T} - \frac{1}{T_0}\right)}$$

Equation 1.5

where β is the material constant known as *beta parameter*, which typically ranges from 3500 and 4600 K depending on the semiconductor material [16]. Most thermistors have a negative temperature coefficient, meaning that their resistance decreases as temperature increases [15]. This behavior allows them to detect small temperature variations with high sensitivity and rapid response times [17]. The high sensitivity can be demonstrated by differentiating Equation (1.5), resulting in:

$$\frac{dR/dT}{R} = -\frac{\beta}{T^2} \quad \text{for } T = 300\,\text{K} \;\Rightarrow\; \frac{dR/dT}{R} = -0.045\ [\text{K}^{-1}]$$

Equation 1.6

However, the same characteristics that make thermistors highly sensitive also limit their applicability. Their operating temperature range is relatively limited, making them unsuitable for high-temperature environments such as combustion systems. Consequently, their use is generally restricted to low-temperature or highly controlled conditions [17].

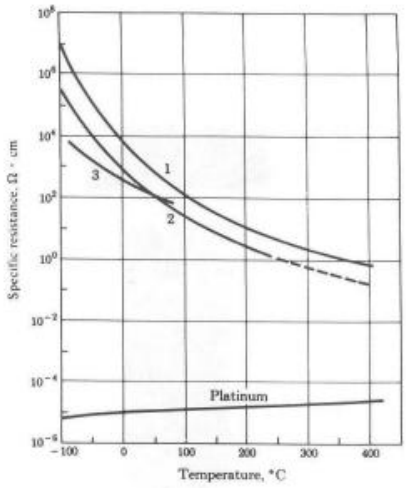

Fig 1.6: *Resistance-temperature characteristics of thermistors and platinum RTDs.* [6]

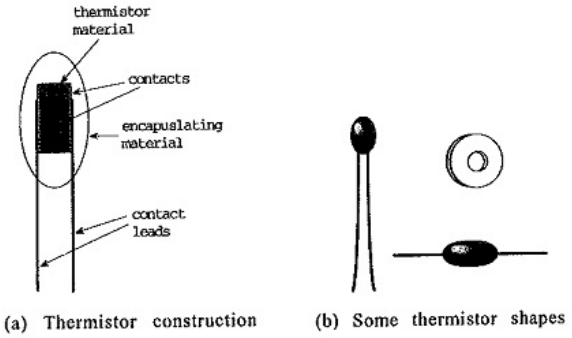

Fig 1.7: *Common thermistor configurations and constructions.* [18]

Fig 1.8: *Aircraft thermistor assembly used for temperature measurements.* [19]

1.4 OPTICAL PYROMETERS

Optical pyrometers are non-intrusive instruments that determine temperature from the thermal radiation emitted by a target [1]. Optical pyrometers can be classified as single-color or two-color instruments, with the latter reducing sensitivity to emissivity variations [20]. These instruments are characterized by very fast responses, very high temperature capabilities (higher than 2000 °C), and by surviving extreme environments since there is no physical contact with the hot gases or components of the engine [1]. However, they are sensitive to emissivity errors, and are affected by soot, oxidation, and the need for a clear optical path, which is not very simple in a jet engine [21].

The energy of thermal radiation emitted by an ideal emitter is a universal function of wavelength and temperature. The spectral distribution of monochromatic emissive power, in units of W/m^2, is [22, 23]:

$$R(\lambda, T) = \frac{C_1}{\lambda^5 \left(e^{\frac{C_2}{\lambda T}} - 1 \right)}$$

Equation 1.7

where C_1 is equal to 3.74 x 10^{-16} Jm^2/s and C_2 is equal to 1.44 x 10^{-2} mK. Planck`s law represents a good approximation of the experimental curves of blackbody emission as a function of wavelength. Temperature is the parameter that characterizes each curve [20, 23].

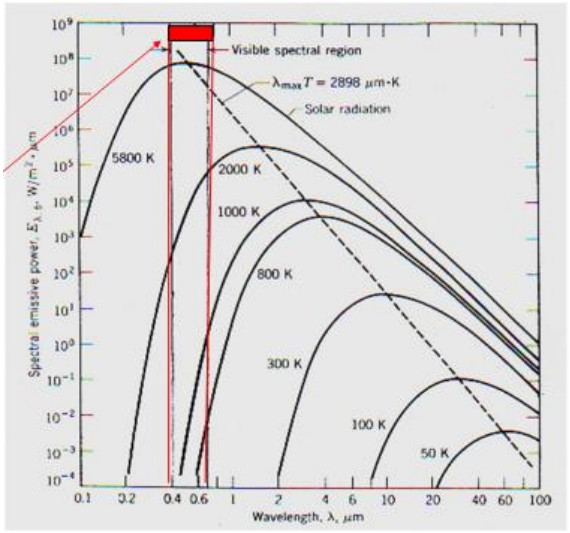

Fig 1.9: *Blackbody radiation curves as a function of wavelength and temperature.* [6]

If we consider, for example, a wavelength of 0.4 micro-meters and a temperature of 5800 Kelvin, we obtain an emissive power of 7.38 x 10^{13} W/m^3 or 7.38 x 10^7 $W/(m^2\mu m)$ according to Equation (1.7), which is consistent with the graph from Figure 1.9. The region highlighted in red, with wavelengths between 0.4 and 0.7 μm, represents the visible light perceived by the human eye [23, 24]. The energy distribution within the spectrum is primarily determined by the temperature of the emitting surface. Any body that emits electromagnetic radiation may be referred to as a radiator [20, 23].

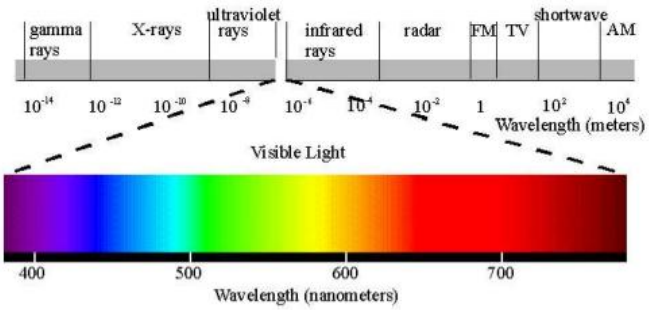

Fig 1.10: *Electromagnetic spectrum showing the visible light region.* [23]

Optical pyrometers measure thermal radiation emitted by a hot object and convert the measured radiation intensity into a temperature value. The instrument is directed toward a target emitting radiation in the visible or infrared spectrum. An optical system consisting of lenses and filters selects a specific wavelength band for analysis [20, 23]. In traditional optical pyrometers, the image of the target is observed together with a reference filament through an eyepiece. By adjusting the electric current supplied to the filament, its brightness can be matched to that of the target. At the point of equal brightness, the filament appears to disappear against the background. The current required to achieve this condition is then related to the temperature of the target [20, 23]. Modern aerospace applications generally replace the human observer with photodetectors that automatically measure radiation intensity [20, 23]. Optical pyrometers measure the brightness temperature rather than the true thermodynamic temperature. Therefore, if emissivity is known, the true temperature can be obtained after corrections [20, 23]. These instruments can be used for exhaust gas temperature (EGT) monitoring, turbine inlet temperature measurements, and combustion-efficiency assessments [1].

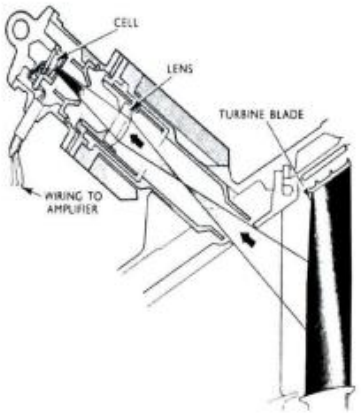

Fig 1.11: *Schematic operating principle of an optical pyrometer.* [23]

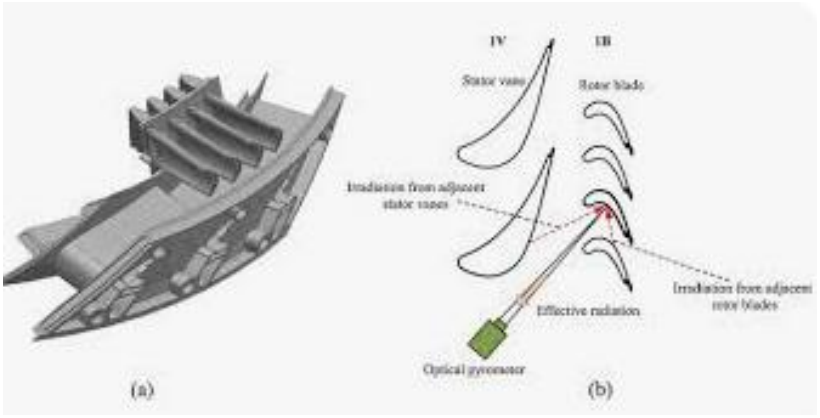

Fig 1.12: *Optical pyrometry applications in gas turbine temperature measurements.* [25]

1.5 THERMAL CAMERAS

Infrared thermography, commonly implemented through thermal cameras, is a non-intrusive measurement technique that extends the principles of optical pyrometry to two-dimensional imaging. These devices detect infrared radiation, typically within the wavelength range of 2-14 μm, and convert it into a spatial temperature distribution [26].

Similar to optical pyrometers, thermal cameras rely on Planck`s law to relate emitted radiation to temperature. The result is a temperature map that provides valuable insight into the thermal behavior of a system [26].

One of the main advantages of thermography is its ability to provide real-time, two-dimensional temperature fields without disturbing the flow. This makes it a powerful diagnostic tool in complex environments [26].

However, its application to burnt gas temperature measurement presents significant challenges. The accuracy of the measurements is strongly influenced by uncertainties in emissivity, which can vary spatially and temporally in combustion gases [20]. Furthermore, thermal cameras measure radiation integrated along the line of sight, rather than a local temperature, which can lead to ambiguities in interpreting the results. For these reasons, thermography is often more suitable for qualitative analysis or surface temperature measurements than for precise gas temperature determination [26].

Fig 1.13: *Handheld infrared thermal imaging camera.* [23]

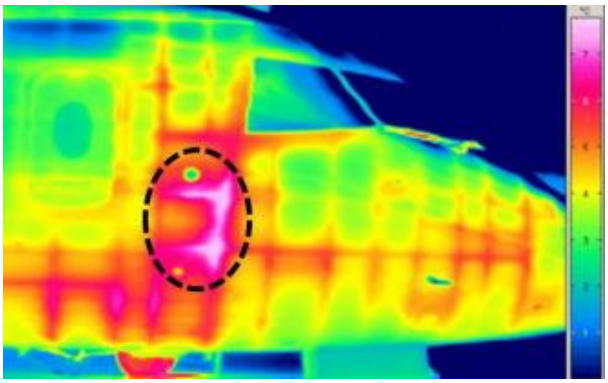

Fig 1.14: *Thermographic image of an aircraft surface obtained using infrared imaging.* [27]

1.6 SUMMARY

The selection of a suitable technique for burnt gas temperature measurement requires a careful balance between measurement range, accuracy, response time, spatial resolution, intrusiveness, environmental sensitivity, and practical implementation.

The table below summarizes the main characteristics of each instrument considered and highlights their suitability for high-temperature combustion measurements.

	T RANGE [DEG C]	INTRUSIVENESS	RESPONSE TIME	ACCURACY	COST	SENSITIVITY	COMPLEXITY
THERMOCOUPLE TYPE K	`-270 to 1260	Intrusive	Fast	`+- 2.2 deg C or +- 0.75%	Low	Medium	Low
THERMOCOUPLE TYPE S	`-50 to 1480	Intrusive	Medium	`+- 1.5 deg C or +- 0.25%	High	Low	Medium
THERMOCOUPLE TYPE R	`-50 to 1480	Intrusive	Medium	`+- 1.5 deg C or +- 0.25%	High	Low	Medium
THERMOCOUPLE TYPE B	`0 to 1700	Intrusive	Medium	`+- 0.50%	Very high	Very low	Medium
THERMOCOUPLE TYPE T	`-270 to 370	Intrusive	Fast	`+- 1.0 deg C or +- 0.75%	Low	Medium-high	Low
THERMOCOUPLE TYPE J	`-210 to 760	Intrusive	Fast	`+- 2.2 deg C or +- 0.75%	Low	Medium	Low
THERMOCOUPLE TYPE E	`-270 to 870	Intrusive	Fast	`+- 1.7 deg C or +- 0.50%	Low	High (best among TC)	Low
RTD	`-200 to 850	Intrusive	Medium	`+- 0.1 deg C	Medium-high	Medium	High
THERMISTOR	`-50 to 150	Intrusive	Very fast	`+- 0.5 deg C	Low	Very high	Medium
OPTICAL PYROMETER	`700 to 3000	Non-intrusive	Very fast	`Medium-high (depends on ε)	High	High	High
THERMAL CAMERA	`-20 to 2000	Non-intrusive	Real-time (very fast)	`+- 2.0 deg C	Very high	High	Very high

Table 1.1: *Comparison of temperature measurement techniques used in combustion and aerospace applications*

Thermocouples provide a robust and versatile solution for high-temperature measurements, offering wide operating ranges and relatively simple implementation. Thermocouples made from noble metals (types S, R, and B) are well suited for extreme temperature conditions, with Type B thermocouples providing the highest temperature capability and excellent stability.

	Wire	
Type	Positive	Negative
S	Platinum	Platinum/ 10% rhodium
R	Platinum	Platinum/ 13% rhodium
B	Platinum/ 30% rhodium	Platinum/ 6% rhodium
T	Copper	Constantan
J	Iron	Constantan
K	Chromel	Alumel
E	Chromel	Constantan

Fig 1.15: *Standard thermocouple types and corresponding materials combinations.* [6]

In contrast, RTDs and thermistors offer high accuracy and sensitivity but are limited by their restricted temperature ranges, making them unsuitable for combustion applications. Non-intrusive techniques such as optical pyrometry and infrared thermography enable measurements without disturbing the flow and allow operation at very high temperatures. However, their accuracy is often limited by uncertainties related to emissivity, radiative transfer, and line-of-sight effects.

Considering these factors, thermocouples represent the most appropriate choice for the present study. Although they are affected by heat transfer mechanisms such as radiation and convection, these effects can be quantified and corrected. Therefore, Type B thermocouple is the instrument selected for the investigation of burnt gas temperature in this work.

CHAPTER 2

COMBUSTION AND THERMAL FIELD FUNDAMENTALS

2.1 INTRODUCTION

Temperature measurement in combustion systems requires knowledge of the physical and chemical processes happening in reacting flows. The temperature field in a flame, for example, is non-uniform and depends on factors such as chemical reactions, heat transfer mechanisms, and flow dynamics [28].

In this work, temperature measurements are performed in a premixed methane-air flame. Therefore, the interpretation of these measurements relies on the understanding of flame structure, temperature distribution, and combustion processes. This chapter introduces the main concepts relevant to the analysis and interpretation of temperature measurements in combustion environments, emphasizing the physical processes that influence flame temperature and its measurement.

2.2 FUNDAMENTALS OF COMBUSTION

Combustion is a chemical process in which fuel reacts with an oxidizer, releasing energy in the form of heat and, in many cases, light [29]. In most engineering applications, the oxidizer is oxygen contained in air, and the process is characterized by explosive (fast) oxidation reactions that convert chemical energy into thermal energy [30].

For the case considered in this study, the fuel is methane (CH_4), and the elementary reaction with oxygen is the following:

$$CH_4 + 2O_2 \rightarrow CO_2 + 2H_2O$$

Equation 2.1

This equation represents the stoichiometric combustion of methane-oxygen mixture, in which methane is fully oxidized to carbon dioxide and water vapor, without leftovers [31]. In practice, air is usually used instead of pure oxygen, introducing nitrogen into the mixture. Even though nitrogen does not participate directly in the reaction, it absorbs part of the released enthalpy (energy) and therefore reduces the final temperature of the combustion products [32].

In addition to heat losses and incomplete mixing, another important phenomenon that affects the final temperature is chemical dissociation. At high temperatures, some of the combustion products partially decompose into simpler species. For example, carbon dioxide and water vapor can dissociate into carbon monoxide and oxygen, and hydrogen and oxygen, respectively [32]:

$$CO_2 \rightleftharpoons CO + \frac{1}{2}O_2$$

Equation 2.2

$$H_2O \rightleftharpoons H_2 + \frac{1}{2}O_2$$

Equation 2.3

These reactions are reversible and become more significant as temperature rises. Dissociation absorbs part of the thermal energy released during combustion, limiting the maximum temperature that can be achieved. As a result, the actual flame temperature is lower than the theoretical value predicted assuming complete combustion without dissociation [32].

The combined effects of nitrogen dilution, heat losses, and dissociation lead to a reduction of the temperature compared to the ideal case. This reduction in temperature leads to reduced thermal efficiency, lower turbine work output (reduced available work), decreased exhaust velocity (decreasing thrust). In summary, dissociation acts as an energy sink that limits the maximum achievable temperature and consequently reduces the efficiency and performance of combustion systems [31]. In the present study, the combustion of a premixed methane-air mixture leads to temperatures that can approach or exceed 2000 °C under near-stoichiometric conditions [33]. In this temperature range, dissociation effects become non-negligible [31].

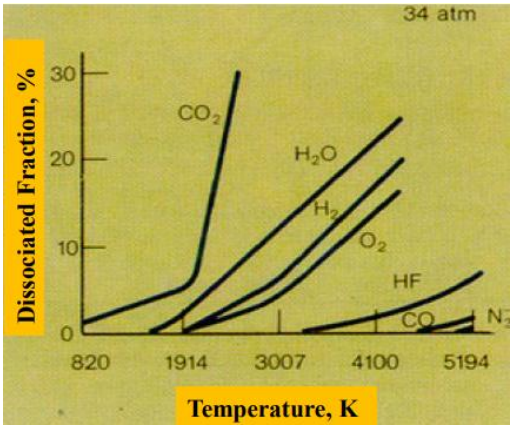

Fig 2.1: *Effect of chemical dissociation on combustion products as a function of temperature.* [32]

Although dissociation reduces the effective temperature and therefore the efficiency and work output, it can also provide certain advantages. Lowering the temperature can reduce the thermal stresses and thermal loading on materials, which is an advantage when considering high-temperature components such as turbine blades. As a result, the durability and lifetime of these components can be improved, which can be a positive tradeoff considering the performance penalties associated with dissociation.

In the context of this work, dissociation is therefore expected to play a role in limiting the maximum temperature measured in the flame and should be considered when comparing experimental results with ideal predictions.

2.3 EQUIVALENCE RATIO AND FLAME TEMPERATURE

An important parameter in combustion analysis is the equivalence ratio, commonly denoted by the Greek letter Φ. This parameter describes the ratio between the actual fuel-air mixture and the stoichiometric mixture (oxidizer-to-fuel ratio is considered here, but the fuel-to-oxidizer ratio can be considered in some cases) [31]:

$$\boldsymbol{\Phi} = \frac{\boldsymbol{O/F}}{\boldsymbol{(O/F)_{Stoichiometric}}}, \text{ and } \Phi = 1 \text{ @ } (O/F)_{Stoichiometric}$$

Equation 2.4

Stoichiometric mixture means that “fuel and oxidizer are fully consumed by the combustion process, which means that there is no excess of fuel or oxidizer in the combustion products” [31]. Therefore, a lean mixture (excess of air or oxidizer) has an equivalence ratio that is less than one, a rich mixture (excess of fuel) has an equivalence ratio that is higher than one, while a stoichiometric mixture has an equivalence ratio equal to one [31].

The equivalence ratio has a strong influence on the flame temperature. Under ideal conditions, the maximum temperature is achieved near stoichiometric conditions and is referred to as the adiabatic flame temperature [34]. This represents the temperature reached by the combustion products, assuming no heat losses to the surroundings.

However, the measured temperature in real systems is always lower than the adiabatic flame temperature due to incomplete combustion, heat transfer to the environment, and chemical dissociation at high temperatures [32]. These effects must be considered when interpreting experimental measurements.

2.4 STRUCTURE OF A PREMIXED FLAME

A premixed flame is characterized by the reactants (fuel and oxidizer) being mixed before ignition, therefore “there is no mass diffusion process occurring” [31]. The resulting flame exhibits a well-defined structure, which can be divided into distinct regions based on temperature and chemical activity.

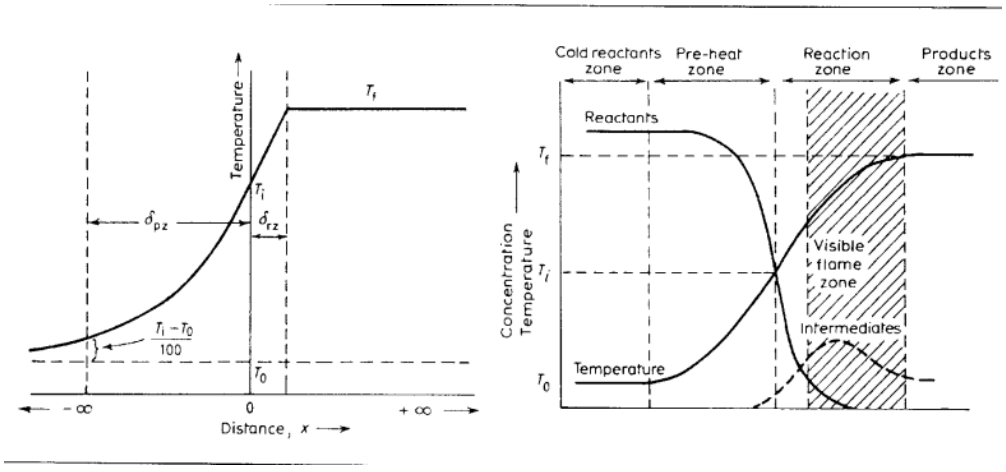

Fig 2.2: *Schematic structure of a premixed flame showing the preheat, reaction, and product zones.* [31]

The main regions of a premixed flame are:

- Preheat zone: in this region, the unburnt mixture is progressively heated due to thermal conduction from the hot burnt gases and, to a lesser extent, by molecular diffusion of energy and reactive species from the reaction zone. Although the mixture is premixed at the macroscopic level, transport processes at the molecular scale still play an important role in the propagation of the flame [31].
- Reaction zone: this is a thin region where the main chemical reactions take place. The temperature rises rapidly, and most of the chemical energy is released. Due to its small thickness, this region presents very steep temperature gradients [31].
- Products zone: in this region, the combustion process is essentially complete. The temperature reaches its maximum value, and the gas composition consists mainly of combustion products [31].

The presence of these distinct regions implies that temperature varies significantly over small spatial scales, making accurate measurements challenging, especially when using intrusive probes.

2.5 TEMPERATURE FIELD IN REACTING FLOWS

In reacting flows, temperature is not always a straightforward quantity to define or measure. While thermodynamic temperature is a well-defined property at equilibrium, practical measurements often depend on the interaction between the measurement device and the surrounding flow [35].

In the case of thermocouples, the measured temperature does not correspond exactly to the true gas temperature. Instead, it represents a balance between different heat transfer mechanisms acting on the sensor, including convection from the gas, conduction within the instrument, and radiation exchange with the surroundings [35].

As a result, the measured values can deviate from the actual gas temperatures, and appropriate corrections must be applied to obtain accurate results. This aspect is particularly relevant in high-temperature environments, where radiative effects become significant [2].

2.6 TEMPERATURE FIELDS IN COMBUSTION SYSTEMS

In practical combustion systems, the temperature field is not uniform and varies both axially and radially [36]. Understanding these spatial variations is important when interpreting temperature measurements because the measured value depends on the location of the probe within the flame.

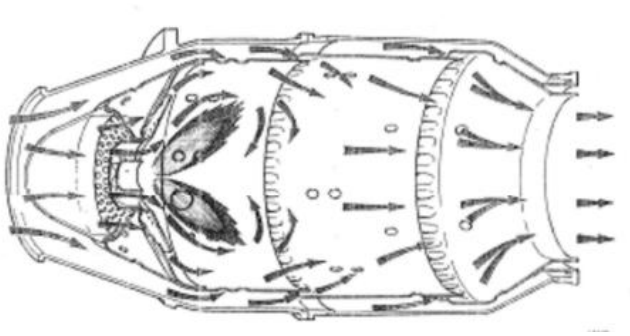

Fig 2.3: *Example of temperature distribution within an aircraft gas turbine combustor.* [37]

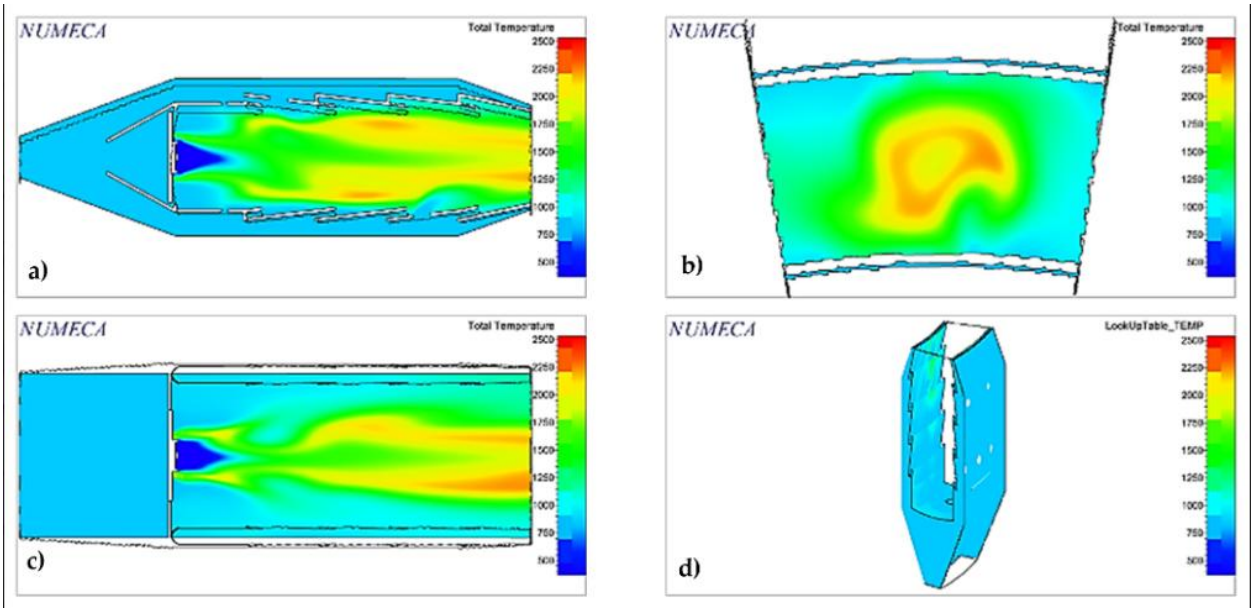

Fig 2.4: *Numerical simulation of temperature contours inside a combustor: (a) midplane in the y-direction; (b) combustor outlet; (c) midplane in the x-direction; (d) isometric view of the flame tube.* [36]

Several factors contribute to the non-uniform radial temperature distribution. Considering the simulation from figure 2.4:

- Central region: the core of the flame typically exhibits higher temperatures due to more efficient mixing and more complete combustion [28].

- Outer region: near the edges of the flame, temperatures are lower due to heat losses to the surroundings and the entrainment of ambient air [28].
- Turbulence effects: turbulent mixing can enhance heat and mass transfer, influencing the shape of the temperature profile [38].
- Boundary effects: interaction with walls or surrounding structures can lead to additional cooling and distortion of the temperature field [28].

Consequently, the measured temperature depends strongly on the measurement location within the flame. Knowledge of the temperature field is therefore important for interpreting experimental results and understanding how representative a local temperature measurement is of the overall combustion process.

2.7 CHALLENGES IN TEMPERATURE MEASUREMENT

Measuring temperature in combustion environments presents several challenges due to the extreme conditions and complex physical phenomena involved. High temperatures, often reaching 2000 °C, can affect sensor materials and measurement accuracy [7].

In addition, combustion gases contain radiating species such as CO_2 and H_2O, which contribute to significant heat transfer. This can lead to measurement errors, especially for intrusive sensors such as thermocouples [2].

Other challenges include turbulence, which introduces temporal fluctuations in temperature, and the presence of strong temperature gradients, which can affect sensor dynamic response. Furthermore, the insertion of a probe into the flow can disturb the local conditions, introducing additional uncertainty [2].

These factors highlight the importance of carefully analyzing and correcting measurement errors in order to obtain reliable temperature data.

2.8 LINK TO PRESENT WORK

In this study, temperature measurements are performed at a selected location within a premixed methane-air flame using a Type B thermocouple. Although the temperature field within the flame is inherently non-uniform, the primary objective of this work is not to

reconstruct the complete temperature distribution, but rather to evaluate the accuracy of thermocouple measurements and quantify the uncertainty associated with the measured temperature.

The following chapters will focus on the experimental setup and the methodology used to acquire the data, as well as on the evaluation of the different sources of error affecting the measurements. Attention is given to calibration uncertainty, quantization effects, radiative heat losses, and dynamic response limitations, with the goal of obtaining a more representative estimate of the true gas temperature.

CHAPTER 3

EXPERIMENTAL SETUP AND METHODOLOGY

3.1 INTRODUCTION

This chapter describes the experimental setup and methodology used to measure the temperature of a premixed methane-air flame using a Type B thermocouple. Attention is given to the configuration of the combustion system, the characteristics of measurement instrumentation, and the procedure adopted to acquire temperature data. The objective is to ensure that the experimental approach is clearly defined and reproducible, while highlighting the main factors that may influence measurement accuracy.

3.2 EXPERIMENTAL FACILITY

The experimental investigation was conducted at CLASD laboratory (Dipartimento di Energia), located in building B13 from Politecnico di Milano La Masa Campus. The combustion test rig was specifically designed for the characterization of premixed methane-air flames and for assessment of temperature measurement techniques in high-temperature combustion environments.

The facility consists of four main subsystems: a methane supply system, a premixed burner and combustion chamber, a thermocouple-based temperature measurement system, and a data acquisition and processing system. A general view of the experimental facility is shown in Figure 3.1.

Fig 3.1: *General view of the experimental facility. (a) Data-acquisition and control system; (b) combustion test rig with burner and thermocouple positioning system*

The test bench includes the burner, the fuel supply line, the thermocouple positioning system, and the electronic instrumentation used for signal acquisition and processing. The experimental setup was originally developed at DENG and has been employed in previous investigations on combustion diagnostics and flame temperature measurements. For the present work, the facility was used to acquire temperature measurements inside a premixed methane-air flame and to assess the accuracy of thermocouple-based temperature measurements.

3.3 PREMIXED BURNER

The combustion system is based on a premixed methane-air burner designed for domestic heating applications. Under nominal operating conditions, the burner delivers a thermal power of approximately 10 kW.

The burner operates according to the Venturi principle. Methane supplied through the fuel line is accelerated through a calibrated nozzle, producing a pressure reduction that induces the entrainment of ambient air into the burner inlet. Air and fuel are mixed upstream of the combustion region, generating a lean premixed combustible mixture.

Combustion takes place at the upper surface of the burner, where a series of rectangular slots provide flame stabilization. The burner head contains 154 pairs of slots measuring 0.85 x 11 mm

and 11 larger slots measuring 0.85 x 24.5 mm. The resulting flame consists of multiple laminar flamelets arranged in a regular pattern over the burner surface.

The equivalence ratio of the mixture depends primarily on the methane flow rate and on the geometric configuration of the Venturi mixing section. By varying the methane flow rate, different operating conditions can be obtained while maintaining stable combustion. A picture of the burner is shown in Figure 3.2, and a picture of the premixed flame is shown in Figure 3.3.

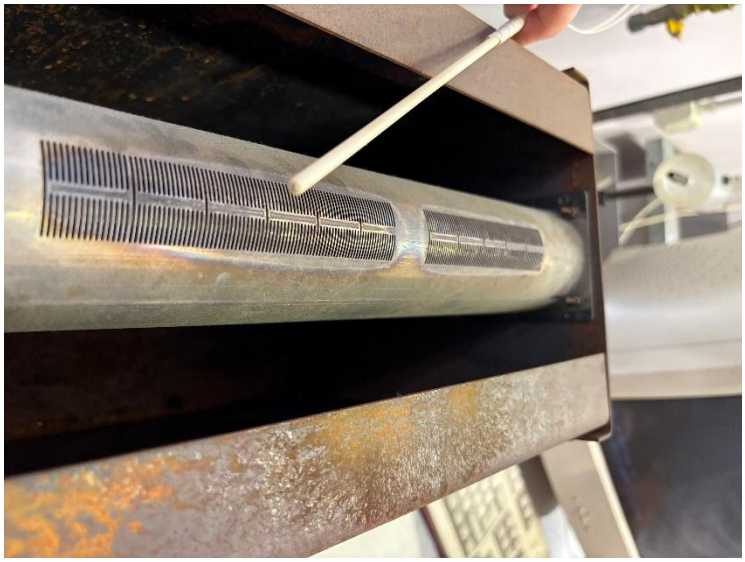

Fig 3.2: *Premixed methane-air burner used in the experimental investigation*

Fig 3.3: *Premixed methane-air flame. (a) Longitudinal view of the flame; (b) transversal view of the flame*

3.4 FUEL SUPPLY SYSTEM

Methane was supplied from the laboratory gas distribution network through a dedicated fuel line connected to the burner nozzle. The fuel flow rate determines the thermal power released by the combustion process and therefore influences the flame temperature field. The methane jet coming from the nozzle generates a pressure drop, which is required for air entrainment within the Venturi section. The resulting premixed mixture flows towards the burner, where combustion occurs. The fuel supply system, including the nozzle and Venturi assembly, is shown in Figure 3.4.

Fig 3.4: *Fuel nozzle and Venturi mixing section used for methane-air premixing.*

3.5 TEMPERATURE MEASUREMENT SYSTEM

3.5.1 THERMOCOUPLE

Temperature measurements were performed using a platinum-rhodium thermocouple. The sensor consists of two wires made of Pt-6%Rh and Pt-30Rh alloys welded together to form the measurement junction. This configuration corresponds to a Type B thermocouple, which is suitable for high-temperature combustion applications because of its excellent repeatability, stability and temperature range of operation.

The thermocouple wires have a diameter of 0.25 mm. The exposed junction configuration minimizes thermal inertia and allows relatively fast response times while maintaining sufficient mechanical strength for operation inside the flame. The thermocouple, as described in section 1.1, measures the junction temperature through the Seebeck effect. The measured electromotive force is converted into temperature using the standard calibration relationship provided for Type B thermocouples. Figure 3.2 shows the thermocouple positioned above the burner.

3.5.2 THERMOCOUPLE POSITIONING SYSTEM

Accurate determination of the temperature field requires precise positioning of the thermocouple inside the flame. The probe was mounted on a three-axis traversing mechanism allowing controlled displacement in the longitudinal, transverse, and vertical directions. The positioning system permits the exploration of the combustion region and enables the acquisition of temperature measurements at predefined spatial locations. The thermocouple positioning system is shown in Figure 3.5.

Fig 3.5: *Three-axis traversing mechanism used for thermocouple positioning.*

3.6 DATA ACQUISITION SYSTEM

The thermocouple signal was acquired through a National Instruments data acquisition system equipped with dedicated signal-conditioning modules. The acquisition system consists of: the thermocouple sensor; a signal-conditioning module with amplification and cold-junction compensation capabilities; an analog-to-digital converter; a personal computer for data storage and processing.

Signal conditioning is necessary to amplify the low-level thermoelectric voltage generated by the thermocouple and to improve the signal-to-noise ratio prior to digitalization. Temperature data were recorded using the acquisition software LabVIEW. The acquisition hardware and conditioning modules are shown in Figure 3.6.

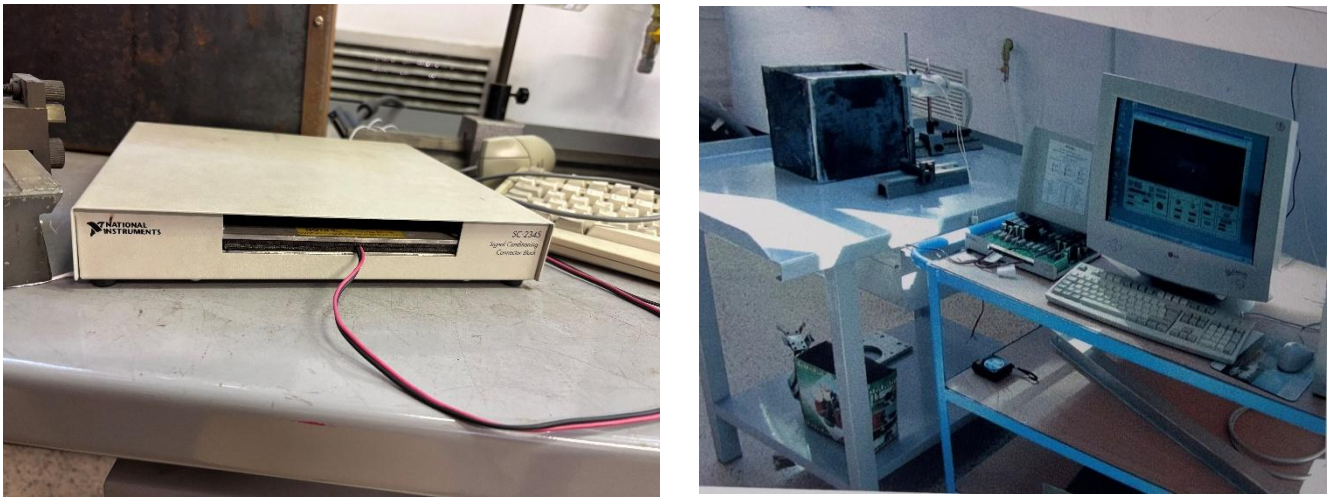

Fig. 3.6: *Data-acquisition system. (a) National Instruments signal-conditioning module; (b) computer workstation used for data acquisition and processing.*

3.7 EXPERIMENTAL PROCEDURE

The objective of the present work is the critical analysis of temperature measurements acquired within a premixed methane-air flame, with the aim of evaluating the discrepancy between the temperature indicated by a Type B thermocouple and the actual gas temperature at the measurement location.

Thermocouple measurements performed in high-temperature environments are affected by several error sources. Radiative heat losses from the hot junction and conductive heat transfer through the thermocouple wires tend to reduce the junction temperature below the true gas temperature. Consequently, the temperature directly measured by the thermocouple generally represents an underestimation of the actual flame temperature.

The experimental measurements are processed through a correction methodology described in Chapter 4, specifically developed to quantify the influence of the dominant error mechanisms. The corrected temperature is therefore considered a more realistic estimate of the true gas temperature than the raw thermocouple reading.

This analysis is highly important in aerospace propulsion applications. The thermal environment experienced by critical engine components, such as turbine blades, directly influences the material selection, cooling-system design, and structural integrity. Designing such components based on uncorrected thermocouple measurements may lead to a dangerous underestimation of the actual thermal loads acting on the structure.

A more accurate estimate of the true gas temperature, obtained by accounting for measurement errors, provides a better representation of the operating environment and contributes to a more reliable assessment of component performance and durability. Therefore, the development and validation of temperature-correction methodologies are essential in combustion diagnostics and high-temperature experimental investigations. The formulation of the thermocouple error models and uncertainty analysis adopted in this work is presented in Chapter 4.

CHAPTER 4

THERMOCOUPLE ERROR MODEL AND UNCERTAINTY ANALYSIS

4.1 OBJECTIVE AND APPROACH

The main objective of this chapter is to present the methodology used to quantify the uncertainty associated with thermocouple temperature measurements and to estimate the corrected gas temperature at the measurement location within the premixed methane-air flame. The measurement techniques and physical background were introduced in the previous chapters. This chapter presents the mathematical formulations implemented in the MATLAB environment to quantitatively evaluate the different sources of error based on the acquired experimental data.

The analysis included the evaluation of the statistical error, systematic error, quantization error, radiative losses, and dynamic behavior of the thermocouple. In addition, a Fourier analysis of the temperature signal is performed in order to investigate the frequency content of the measured thermal fluctuations and identify possible oscillatory or turbulent phenomena occurring within the flow.

The analysis is carried out at the measurement location investigated during the experiments. The objective is to determine the corrected gas temperature and its associated uncertainty by accounting for the dominant error mechanisms affecting the thermocouple measurements.

4.2 STATISTICAL ERROR

Statistical errors are random and related to fluctuations that are found when repeating measurements with an instrument. Statistical analysis is performed using a given sample, and important parameters such as variance and standard deviation need to be calculated in order to quantify the statistical error.

In the present work, two sets of temperature measurements were obtained were obtained at the selected measurement location. The first set is called “prova low number” and has 1200 samples, while the second one is called “prova high number” and has 9000 samples. For both sets of data, the sampling rate was defined as 0.01 seconds (sampling frequency of 100 Hz), which means that the system is capturing one hundred samples per second, which is excellent for dynamic testing. The statistical analysis step by step is described below.

The samples are separated into different classes of temperature, which are composed of a minimum and a maximum temperature value. The number of classes or bins (k) is dependent on the number of samples (N), and can be defined by the Sturge`s law [39]:

$$k = 1 + 3.322 \log_{10}(N)$$

Equation 4.1

Then, the class size is defined by dividing the difference between the maximum and minimum temperature of the data by the number of bins, and therefore the minimum and maximum temperatures of each class can be defined. With the classes defined, the class occurrence frequency, which is simply the number of data points that fall within each class, can be obtained. The class occurrence frequency is important because it shows how often a temperature value occurs and it allows a representation of the probability distribution of the measured temperature signal through a histogram and the presence of fluctuations.

The mean temperature is calculated by summing all the data points and dividing by the total number of samples. The mean temperature is important for the calculation of a key parameter in statistical analysis: the variance. The variance gives an idea of how strong the temperature fluctuations are, it gives emphasis on larger deviations, and it is mathematically described by being the mean squared deviation of the measured temperature from its mean value. The variance formula is given below [40]:

$$\sigma^2 = \frac{1}{N-1}\sum_{i=1}^{N}(T_i - \overline{T})^2$$

Equation 4.2

where N is the number of samples, and T_i is each individual temperature value.

Another important parameter in statistical analysis is the standard deviation, which is the square root of the variance. The units for variance and standard deviation are $°C^2$ (or K^2) and °C, respectively. The standard deviation can be physically interpreted as the usual magnitude of fluctuations. For example, if the standard deviation is 10 °C, it means that the signal has a typical deviation of 10 °C from the mean value [40].

The statistical error has the following formula [41]:

$$\varepsilon_{\text{stat}} = t_{\nu^o, P\%}\frac{\sigma}{\sqrt{N}}$$

Equation 4.3

Where σ is the standard deviation, N is the number of samples, and t is the Student`s t-distribution, with $\nu^o$ and P% representing the degrees of freedom and the confidence level, respectively. The Student`s t-distribution is a probability distribution used to estimate the mean value of a dataset, accounting for the uncertainty, and it depends on the number of degrees of freedom and the selected confidence level.

Degrees of freedom ν	t_{50}	t_{80}	t_{90}	t_{95}	t_{98}	t_{99}	$t_{99.9}$
1	1.000	3.078	6.314	12.706	31.821	63.657	636.619
2	0.816	1.886	2.920	4.303	6.965	9.925	31.598
3	0.765	1.638	2.353	3.182	4.541	5.841	12.941
4	0.741	1.533	2.132	2.776	3.747	4.604	8.610
5	0.727	1.476	2.015	2.571	3.365	4.032	6.859
6	0.718	1.440	1.943	2.447	3.143	3.707	5.959
7	0.711	1.415	1.895	2.365	2.998	3.499	5.405
8	0.706	1.397	1.860	2.306	2.896	3.355	5.041
9	0.703	1.383	1.833	2.262	2.821	3.250	4.781
10	0.700	1.372	1.812	2.228	2.764	3.169	4.587
11	0.697	1.363	1.796	2.201	2.718	3.106	4.437
12	0.695	1.356	1.782	2.179	2.681	3.055	4.318
13	0.694	1.350	1.771	2.160	2.650	3.012	4.221
14	0.692	1.345	1.761	2.145	2.624	2.977	4.140
15	0.691	1.341	1.753	2.131	2.602	2.947	4.073
16	0.690	1.337	1.746	2.120	2.583	2.921	4.015
17	0.689	1.333	1.740	2.110	2.567	2.898	3.965
18	0.688	1.330	1.734	2.101	2.552	2.878	3.922
19	0.688	1.328	1.729	2.093	2.539	2.861	3.883
20	0.687	1.325	1.725	2.086	2.528	2.845	3.850
21	0.686	1.323	1.721	2.080	2.518	2.831	3.819
22	0.686	1.321	1.717	2.074	2.508	2.819	3.792
23	0.685	1.319	1.714	2.069	2.500	2.807	3.767
24	0.685	1.318	1.711	2.064	2.492	2.797	3.745
25	0.684	1.316	1.708	2.060	2.485	2.787	3.725
26	0.684	1.315	1.706	2.056	2.479	2.779	3.707
27	0.684	1.314	1.703	2.052	2.473	2.771	3.690
28	0.683	1.313	1.701	2.048	2.467	2.763	3.674
29	0.683	1.311	1.699	2.045	2.462	2.756	3.659
30	0.683	1.310	1.697	2.042	2.457	2.750	3.646
40	0.681	1.303	1.684	2.021	2.423	2.704	3.551
60	0.679	1.296	1.671	2.000	2.390	2.660	3.460
120	0.677	1.289	1.658	1.980	2.358	2.617	3.373
∞	0.674	1.282	1.645	1.960	2.326	2.576	3.291

Fig 4.1: *Student`s t-distribution critical values for different confidence levels and degrees of freedom* [41]

For example, if I have 9000 samples in a dataset, the number of degrees of freedom is 8999. In addition, a confidence level of 95% is adopted in this work, which represents a compromise between statistical reliability and uncertainty related to experimental measurements. From Figure 4.1, considering the degrees of freedom for the 9000 samples and the selected confidence level, the value of t is 1.96.

4.3 SYSTEMATIC ERROR

Systematic errors, or bias errors, are consistent deviations from the “true” temperature value and are usually caused by heat conduction and radiation. In order to estimate the systematic error of the thermocouple, a static calibration was performed, yielding 21 voltage measurements and their corresponding temperature values. With this data, a linear regression analysis using the least squares method was performed with the goal of determining the best-fit line that minimized the sum of the squared differences between the actual data points and the predicted values. The linear equation is represented as [42]:

$$y = A + Bx \quad \text{or} \quad y = A_1 + B(x - \bar{x})$$

Equation 4.4

where y is the dependent variable (temperature, in degrees Celsius), x is the independent variable (voltage, in millivolts), A is the intercept of the regression line, B is the slope of the regression line, A_1 is the mean value of y, and x bar is the mean value of x. The formula for obtaining the slope of the regression line is [42]:

$$B = \frac{\sum_{i=1}^{21} (x_i - \bar{x})\, y_i}{\sum_{i=1}^{21} (x_i - \bar{x})^2}$$

Equation 4.5

Finally, the intercept of the regression line is found by equating both equations from Equation 4.4, which results in [42]:

$$A = A_1 - B\bar{x}$$

Equation 4.6

Once the linear correlation is obtained, one important parameter to calculate and understand the accuracy and reliability of the calibration is called coefficient of determination (R^2), and it has the following equation [42]:

$$R^2 = \frac{\sum_{i=1}^{N} (\hat{y}_i - \bar{y})^2}{\sum_{i=1}^{N} (y_i - \bar{y})^2}$$

Equation 4.7

The numerator of the equation above is the sum of the difference between predicted values from the linear regression (from Equation 4.4) and the mean value of the experimental values squared, and the denominator is the sum of the difference between the experimental values and the mean value of the experimental values squared. A coefficient of determination close to 1 represents a very good fit, while a coefficient close to 0 represents a poor fit.

To calculate the standard error of regression, the standard deviation associated with the interpolation (or regression) error needs to be obtained. Similarly to the definition in the case of statistical error, the standard deviation in this case represents the typical deviation, and therefore uncertainty, between the experimental measurements and the predicted values by the regression model, and the formula is [42]:

$$\sigma_\varepsilon = \sqrt{\frac{\sum_{i=1}^{N}(y_i - \hat{y}_i)^2}{N-2}}$$

Equation 4.8

In this case, the denominator is "N – 2" because two parameters are estimated in linear regression: the slope B and the intercept A. Therefore, the denominator represents the number of degrees of freedom left.

The systematic error of the thermocouple also depends on the Student`s t distribution, which was explained at section 4.2. With a confidence level of 95%, and 19 degrees of freedom (N – 2), the value of t is 2.09 from Figure 4.1, and the systematic error of the thermocouple is found by multiplying the t-factor with the standard deviation [42]:

$$\varepsilon_{\text{sist}} = t_{\nu^\circ,\, P\%}\, \sigma_\varepsilon$$

Equation 4.9

The linear regression was compared to other interpolation models with polynomials of higher degrees in order to understand if more complex models provided a better representation of experimental data. Sometimes a set of data can present nonlinear behaviors that are not accurately captured by linear equations, so higher-order models may be necessary, especially in calibration curves.

The comparison was performed by analyzing the interpolation standard deviation for each polynomial fit. A lower value of σ_ε indicates that the regression curve follows the experimental data with higher precision. Equation 4.8 is modified [43]:

$$\sigma_\varepsilon = \sqrt{\frac{\sum_{i=1}^{N}(y_i - \hat{y}_i)^2}{N - (m+1)}}$$

Equation 4.10

with m representing the polynomial degree, and the denominator corresponding to the remaining degrees of freedom.

Polynomials up to the fourth order were compared and the model with the lowest standard deviation was adopted, and the systematic error was calculated using Equation 4.9. The systematic error or the sample instrument, which represents the uncertainty of the instrumentation and calibration system, must also be considered. It is usually provided by the manufacturer, and in this case the value of 0.50% of the full scale was adopted. Finally, the total systematic error of the thermocouple is [42]:

$$\varepsilon_{\text{sist-total}} = \sqrt{\varepsilon_{\text{sist}}^2 + \varepsilon_{\text{sist-sample instrument}}^2}$$

Equation 4.11

4.4 QUANTIZATION ERROR

Quantization errors are instrumentation errors that are encountered in the process of data acquisition. In order to quantify this error related to data acquisition, a time series measurement of the voltage signal of the type B thermocouple was performed. The 28 values obtained are expressed in V, with the original signal being amplified by a factor of 100, and the signal was acquired by a card with a 12-bit analog-to-digital (A/D) converter with range 0 to 10 V. Their respective temperature values were also obtained.

The quantization error depends only on the features of the A/D converter board. It has the following formula (in V) [44]:

$$\varepsilon_{\text{quant}} = \frac{0.5\,F}{2^n}$$

Equation 4.12

where F is the full-scale voltage range (10 in this case), and n is the number of A/D bits (12 in this case). To estimate the total quantization error, it is necessary to convert from V to °C, using the following formula [44]:

$$\varepsilon_{\text{quant}} = \left(\frac{0.5\,F}{2^n}\right)\left(\frac{dy}{dx}\right)$$

Equation 4.13

where dy/dx is the error propagation, which is calculated by dividing the difference of the maximum and minimum temperature values by the difference between the maximum and minimum voltage values obtained in the time series measurement.

4.5 THERMOCOUPLE RADIATION LOSSES

The temperature measured by the thermocouple corresponds to the temperature of the sensor, or the temperature of the hot junction since the cold junction is in a reference condition. The indicated temperature by the sensor does not match the gas temperature because errors originated by several factors, including conduction and radiation. Conduction errors can be minimized by

making the ratio of the wire cross-sectional area and their length as small as possible and therefore are usually neglected. The thermal radiation involved in thermocouple measurements is often the dominant error source, and it is caused by the electromagnetic radiation emitted by the combustion gases due to their high temperature [45].

In order to estimate the radiative losses, an energy balance at the thermocouple hot junction is performed under steady-state conditions. The equation below can be read as: the thermal power entering the hot junction through convective heat transfer from the hot gases must be equal to the net radiative power exchanged between the thermocouple and the surrounding environment [45]:

$$h(T_{gas} - T_g) = \sigma\varepsilon(T_g^4 - T_a^4)$$

Equation 4.14

where h is the convective heat transfer coefficient, T_{gas} is the gas temperature (unknown), T_g is the junction temperature (measured by the thermocouple), T_a is the ambient temperature (sometimes called T_{wall}, or wall temperature), ε is the thermocouple emissivity, and σ is the Stefan-Boltzmann constant.

From Equation 4.14, the radiative loss of the thermocouple to the wall can be written as [45]:

$$\Delta T_{rad} = T_{gas} - T_g = \frac{\sigma\varepsilon(T_g^4 - T_a^4)}{h}$$

Equation 4.15

The only unknown of this equation is the gas temperature. However, determining the convective heat transfer coefficient and the thermocouple emissivity is not simple. Considering the thermocouple junction as a wire exposed to a high-temperature fluid, a semi-empirical correlation is used to determine the parameter h [45]:

$$Nu = \frac{hD}{k} = CRe^n Pr^m$$

Equation 4.16

where Nu is the Nusselt number, which is a dimensionless number that represents the ratio between convective and conductive heat transfer, D is the junction diameter, k is the thermal conductivity of the flow surrounding the thermocouple junction, Re is the Reynolds number, which is a dimensionless number that represents the ratio between inertial and viscous forces, and Pr is the Prandtl number, which is a dimensionless number that represents the ratio between momentum diffusivity and thermal diffusivity. The coefficient m is very close to 0 in the Reynolds number range 1 to 35, and therefore the Prandtl number is unity in this case, indicating that the influence of Pr on the convective heat transfer correlation is negligible. The coefficients C and n vary with the Reynolds number, which is calculated by the following equation [45]:

$$Re = \frac{vD}{\nu}$$

Equation 4.17

where v is the flow velocity, and ν is the kinematic viscosity of the combustion gases, which represents the ratio between the fluid`s dynamic viscosity and its density. Under these conditions, coefficients C and n can be approximated as 0.80 and 0.38, respectively [45].

The measurements were performed using a Type B thermocouple that has an exposed junction with a diameter of 0.25 mm and emissivity equal to 0.20, which means that the junction emits only 20% of the thermal radiation that an ideal blackbody would emit at the same temperature, and therefore the radiative heat losses of the thermocouple are lower than highly emissive surfaces.

The correlation of Figure 4.16, as mentioned previously, is valid only within a limited Reynolds number range. At higher velocities, the Reynolds number may exceed the correlation limits, and therefore other correlations must be used. The Churchill-Bernstein correlation, which provides reliable predictions for convective heat transfer around cylinders (good approximation for thermocouples) over a broad range of flow regimes, including laminar and turbulent conditions, is the one chosen for this work. This correlation has a wide validity range, it is frequently used in combustion problems and thermocouple correction studies, and it is shown below [46]:

$$Nu = 0.3 + \frac{0.62 Re^{1/2} Pr^{1/3}}{\left[1 + \left(\frac{0.4}{Pr}\right)^{2/3}\right]^{1/4}} \left[1 + \left(\frac{Re}{282000}\right)^{5/8}\right]^{4/5}$$

Equation 4.18

The step by step for calculating the radiative losses of the thermocouple is an iterative procedure. For each set of data obtained from measuring the gas temperature at different radius, the mean value is considered as the temperature of the junction (T_g), and the wall temperature (surrounding temperature) was considered equal to 293 K (20 °C). The constants such as junction diameter and Stefan-Boltzmann constant are defined, and two loops are started: one for the emissivity varying from 0.20 to 0.80 and the other for the flow velocity varying from 1 to 100 m/s. It is important to mention that the emissivity of the thermocouple can increase with the use of the instrument, which is exposed to extremely high temperatures. The surface properties of the junction can be modified during operation as a result of oxidation, surface roughening, and deposits from combustion products. Consequently, thermal radiation emission increases and the emissivity increases, which leads to greater radiative heat losses [45].

For each value of emissivity, the MATLAB code iteratively computes the radiative losses for each gas velocity, which is another loop inside the emissivity loop. As an example, the case where thermocouple emissivity is 0.20 and the gas velocity is 1 m/s is considered below. The initial guess for starting the iteration is that the temperature of the gas is equal to the temperature of the hot junction, and the film temperature, which is the average temperature between the surface and the surrounding fluid, is used to evaluate the thermophysical properties of the flow. A MATLAB function is called to interpolate the thermophysical properties of the flow at the film temperature, such as density, thermal conductivity, Prandtl number, etc. With the properties of the flow, the Reynolds number can be calculated and used to calculate the Nusselt number using Equation 4.16 or Equation 4.18, depending on the value of Reynolds. At this point, Equation 4.16 is inverted to obtain the convective heat transfer coefficient (h), which is the last unknown from the energy balance at the hot junction of the thermocouple (Equation 4.14). Finally, the "new" gas temperature is calculated and checked with the assumption made at the beginning of the iteration, up to convergence. The difference between the gas temperature and the temperature

of the junction is the radiative loss of the thermocouple, and this value is recorded for each flow velocity (1 – 100 m/s) at each value of emissivity considered (0.20 – 0.80).

4.6 THERMOCOUPLE DYNAMIC ANALYSIS

The dynamic analysis of the thermocouple is essential to evaluate the capability of the sensor to follow rapid temperature variations occurring in the combustion process. Due to its finite thermal inertia, the thermocouple does not respond instantaneously to changes in the gas temperature, which may lead to attenuation and delay of the measured signal. This effect becomes particularly important in fluctuating or turbulent flows, where temperature variations may occur on time scales comparable to the sensor response time [47]. An excessive dynamic delay may lead to an underestimation of rapid temperature peaks, which is a critical aspect in gas turbine applications. The first turbine stages, for example, are subjected to the highest thermal loads and must operate below the melting temperature and allowable thermal limits of the blade material. Accurate temperature monitoring is therefore fundamental in order to prevent thermal overstressing, material degradation, and possible structural failure. For this reason, a dynamic calibration of the thermocouple was performed to estimate its characteristic time constant and assess the dynamic behavior of the sensor.

The analysis was carried out using the dynamic calibration signal acquired experimentally. The temperature signal was first imported into MATLAB together with the corresponding sampling time, allowing the construction of the temporal evolution of the measured temperature. The raw calibration signal was then plotted to visualize the transient response of the thermocouple.

To characterize the sensor dynamics, the thermocouple was modeled as a first-order system. The initial temperature T_0 was taken as the first value of the transient, while the steady-state temperature T_∞ was estimated as the average of the final samples of the signal. A dimensionless response function was then introduced to describe the transient evolution of the thermocouple response [47]:

$$\Gamma = \frac{T(t) - T_\infty}{T_0 - T_\infty}$$

Equation 4.19

where T(t) is the instantaneous thermocouple temperature. This dimensionless parameter represents the relative distance of the thermocouple response from equilibrium during the transient process. For an ideal first-order system, the response decreases exponentially with time, approaching zero as the thermocouple reaches thermal equilibrium. The evolution of Γ therefore characterizes the dynamic behavior of the sensor and allows the estimation of the thermocouple time constant. The theoretical solution is [47]:

$$\Gamma = e^{-t/\tau_c}$$

Equation 4.20

where τ_c is the thermocouple time constant.

In order to determine the time constant experimentally, only physically meaningful values satisfying $0 < \Gamma < 1$ were retained, excluding noisy or nonphysical points. A logarithmic transformation was then applied [47]:

$$\ln(\Gamma) = -\frac{t}{\tau_c}$$

Equation 4.21

This transformation converts the exponential decay into a linear relation, allowing the use of linear regression through the least-squares method. A MATLAB function called “polyfit” was used to determine the slope of the linear fit, from which the thermocouple time constant was obtained as [47]:

$$\tau_c = -\frac{1}{\text{slope}}$$

Equation 4.22

Once the time constant was estimated, the first-order model of the thermocouple response was reconstructed and compared with the experimental measurements. Additional plots of the

dimensionless response Γ and of the logarithmic regression were generated in order to validate the first-order approximation and evaluate the quality of the fitting procedure.

The obtained time constant provides a quantitative measure of the thermocouple dynamic response and allows the assessment of possible dynamic errors associated with transient temperature measurements.

For a first-order thermocouple response, the time constant represents the characteristic response time of the sensor. However, the thermocouple reaches approximately 99% of the final temperature only after a time interval of about 5 times the time constant. Consequently, rapid thermal transients occurring on shorter time scales may not be accurately detected, leading to attenuation and delay of the measured temperature signal. This aspect is critical in combustion and gas turbine applications, where accurate monitoring of peak temperatures is essential to prevent possible damage to turbine components due to excessive thermal loading [47].

4.7 FOURIER ANALYSIS OF THE TEMPERATURE SIGNAL

In addition to the uncertainty and dynamic analyses, a Fourier analysis of the thermocouple signal was performed in order to investigate the frequency content of the measured temperature fluctuations. The objective of this analysis is to identify dominant oscillation frequencies associated with turbulence, combustion instabilities, or periodic thermal phenomena occurring within the flame. The frequency-domain analysis allows the evaluation of the thermocouple dynamic response, since the finite sensor time constant may attenuate high-frequency temperature fluctuations.

The analysis was carried out using the experimental dataset acquired with the Type-B thermocouple. The sampling frequency, which was defined as the inverse of the sampling time, represents the number of acquired samples per second and defines the maximum frequency that can be resolved through the Fourier analysis.

Before performing the spectral analysis, the mean temperature value was removed from the signal [48]:

$$T_{fluct}(t) = T(t) - \overline{T}$$

Equation 4.23

where T(t) is the instantaneous measured temperature, and $\overline{T}$ is the mean temperature value.

This operation isolates the fluctuating component of the signal and eliminates the dominant constant contribution corresponding to the average temperature. Without this preprocessing step, the Fourier spectrum would be dominated by a large peak at zero frequency, making the identification of the physically relevant oscillatory components more difficult [49].

The Fast Fourier Transform (FFT) algorithm was subsequently applied to the fluctuating temperature signal. The FFT converts the signal from the time domain into the frequency domain, allowing the decomposition of the temperature fluctuations into sinusoidal components characterized by different frequencies and amplitudes. Each spectral component represents the contribution of a specific oscillation frequency to the overall signal. Mathematically, the discrete Fourier transform can be expressed as [50]:

$$Y(k) = \sum_{n=0}^{N-1} T_{\text{fluct}}(n) e^{-j\frac{2\pi kn}{N}}$$

Equation 4.24

where (N) is the total number of samples, k is the frequency index, and j is the square root of (-1).

The complex Fourier coefficients obtained from the FFT were then converted into amplitude values through normalization with respect to the number of samples [50]:

$$P_2(k) = \left| \frac{Y(k)}{N} \right|$$

Equation 4.25

where Y represents the Fourier transform of the signal, N is the total number of samples, and P2 is referred to as the two-sided amplitude spectrum because it contains both the positive and negative frequencies. This characteristic originates from the mathematical formulation of the Fourier transform, in which each sinusoidal component can be represented by two symmetric complex exponential terms at frequencies +f and -f. For real-valued physical signals, such as the

thermocouple temperature signal, the spectrum is symmetric with respect to zero frequency. Consequently, the information contained in the negative-frequency region is redundant from a physical viewpoint [50].

For this reason, only the positive-frequency portion of the spectrum was retained, generating the so-called one-sided spectrum P1. In order to conserve the total signal energy, the amplitudes of all frequency components except the zero-frequency contribution were multiplied by a factor of two [50]:

$$P_1(k) = 2P_2(k) \qquad k = 2, \ldots, \frac{N}{2}$$

Equation 4.26

The resulting one-sided spectrum therefore provides a physically meaningful representation of the amplitudes associated with the real oscillatory components of the temperature signal.

The frequency vector associated with the spectrum was then constructed according to [50]:

$$f = \frac{f_s}{N}(0, 1, 2, \ldots, N/2)$$

Equation 4.27

allowing each spectral amplitude to be associated with its corresponding physical frequency.

The frequency resolution of the analysis is determined by [50]:

$$\Delta f = \frac{f_s}{N}$$

Equation 4.28

where Δf represents the minimum frequency interval that can be distinguished within the spectrum. A larger acquisition time, corresponding to a greater number of samples, results in improved frequency resolution and allows lower-frequency oscillatory phenomena to be

identified. The highest frequency that can be correctly reconstructed is the Nyquist frequency [50]:

$$f_N = \frac{f_s}{2}$$

Equation 4.29

which represents the upper limit of the measurable frequency range. Frequency components above this limit cannot be accurately reconstructed and may generate aliasing effects, producing flawed contributions at lower frequencies. Therefore, the sampling frequency must be selected so that all physically relevant oscillations remain below the Nyquist limit.

The obtained spectrum was finally plotted as a function of frequency. In order to improve the visualization of the smaller spectral components and facilitate the identification of dominant frequencies, a logarithmic scale was adopted for the amplitude axis. This representation is particularly useful when a few dominant peaks coexist with a broad distribution of lower-amplitude fluctuations [50].

The resulting frequency spectrum provides valuable information regarding the temporal scales characterizing the combustion process. Sharp peaks in the spectrum indicate periodic or quasi-periodic oscillations that may be associated with combustion instabilities, acoustic resonances, vortex shedding, or other organized flow phenomena. On the other hand, broadband spectral distributions are generally associated with stochastic processes such as turbulence and random fluctuations of the flame structure [50].

The Fourier analysis therefore complements the statistical, uncertainty, and dynamic analyses presented in the previous sections. While quantities such as the mean temperature, standard deviation, and uncertainty characterize the overall quality of the measurement, the frequency-domain representation reveals the temporal structure of the temperature fluctuations and enables the identification of the dominant mechanisms governing the thermal field within the combustion region.

4.8 SUMMARY

This chapter presented a comprehensive analysis of the uncertainties and error sources affecting the temperature measurements performed with the Type-B thermocouple. Statistical, systematic, and quantization errors associated with the measurement were evaluated to quantify their contribution to the overall uncertainty.

Attention was given to thermocouple-specific effects. Radiative heat losses from the sensing junction were identified as a major source of temperature underestimation in the high-temperature combustion environment investigated. In addition, the dynamic response of the thermocouple was analyzed to assess its ability to accurately track temperature fluctuations. A Fourier analysis of the acquired signals was then performed to investigate the frequency content of the measured temperature field and to evaluate the influence of sensor dynamics on the recorded fluctuations.

The methodologies and formulations developed in this chapter provide the basis for correcting the measured temperatures and for assessing the reliability of the experimental data. In the next chapter, the measured and corrected temperature distributions are presented and discussed, including the implications of the identified error mechanisms on the characterization of the methane-air premixed flame.

CHAPTER 5

RESULTS AND DISCUSSION

5.1 STATISTICAL ANALYSIS OF THE TEMPERATURE SIGNAL

5.1.1 ANALYSIS OF THE 1200-SAMPLE DATASET

In this section, the statistical properties of the temperature signal acquired using 1200 samples are evaluated, following the steps described in chapter 4.2. The measurement was performed with a sampling frequency of 100 Hz, corresponding to a total acquisition time of 12 seconds.

The number of classes was calculated using Sturge`s law (Equation 4.1), and it is equal to 11. The following table shows the start and end temperature values for each class, with their class occurrence frequency and cumulative frequency of occurrence.

Start	End	Class Occurrence Frequency	Class Occurrence Frequency %	Cumulative Frequency of Occurrence	Cumulative Frequency of Occurrence
953.75	975.29	9	0.75	9	0.75
975.29	996.84	20	1.6667	29	2.4167
996.84	1018.4	54	4.5	83	6.9167
1018.4	1039.9	112	9.3333	195	16.25
1039.9	1061.5	230	19.167	425	35.417
1061.5	1083	195	16.25	620	51.667
1083	1104.6	293	24.417	913	76.083
1104.6	1126.1	174	14.5	1087	90.583
1126.1	1147.7	80	6.6667	1167	97.25
1147.7	1169.2	25	2.0833	1192	99.333
1169.2	1190.7	8	0.66667	1200	100

Table 5.1: *Statistical classes and occurrence frequencies for the 1200-sample dataset.*

The modal class, which represents the most frequent temperature values, is the one from 1083.00 to 1104.60 °C. The mean temperature value is 1077.20 °C, the variance is 1535.60 °C^2, and the standard deviation is 39.20 °C. Finally, the absolute statistical error is 2.22 °C, and the histogram is shown below:

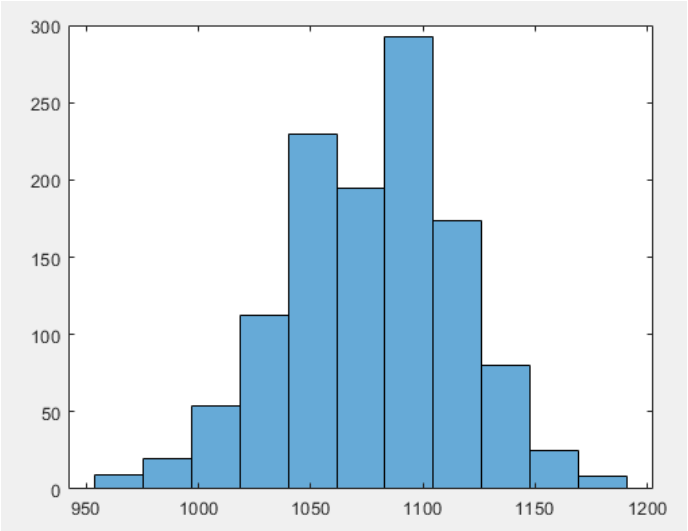

Fig 5.1: *Temperature histogram for the 1200-sample dataset.*

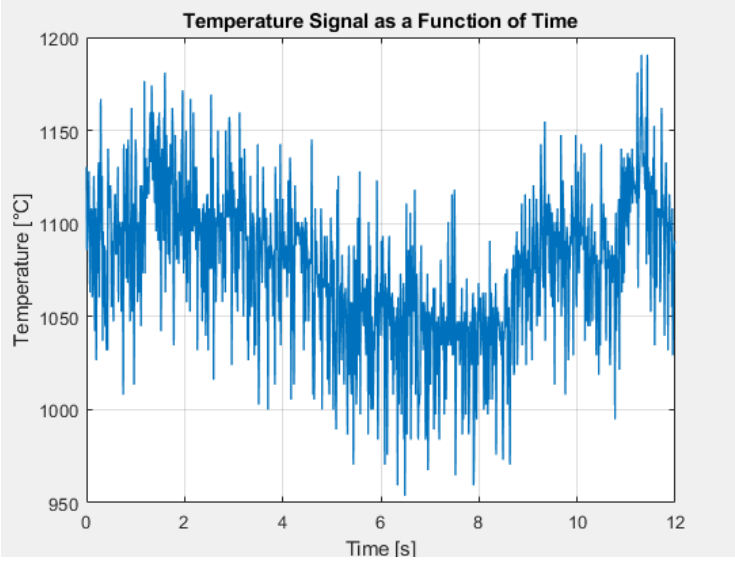

Fig 5.2: *Temperature signal as a function of time for the 1200-sample dataset.*

5.1.2 ANALYSIS OF THE 9000-SAMPLE DATASET

The statistical properties of the temperature signal acquired using 9000 samples are now evaluated. In this case, having the same sampling frequency, the total acquisition time was 90 seconds.

The number of classes in this case is 14. The following table shows the start and end temperature values for each class, with their class occurrence frequency and cumulative frequency of occurrence.

Start	End	Class Occurrence Frequency	Class Occurrence Frequency %	Cumulative Frequency of Occurrence	Cumulative Frequency of Occurrence %
931.35	968.39	18	0.2	18	0.2
968.39	1005.4	108	1.2	126	1.4
1005.4	1042.5	400	4.4444	526	5.8444
1042.5	1079.5	918	10.2	1444	16.044
1079.5	1116.6	1610	17.889	3054	33.933
1116.6	1153.6	1925	21.389	4979	55.322
1153.6	1190.6	1611	17.9	6590	73.222
1190.6	1227.7	937	10.411	7527	83.633
1227.7	1264.7	595	6.6111	8122	90.244
1264.7	1301.8	488	5.4222	8610	95.667
1301.8	1338.8	189	2.1	8799	97.767
1338.8	1375.8	121	1.3444	8920	99.111
1375.8	1412.9	72	0.8	8992	99.911
1412.9	1449.9	8	0.088889	9000	100

Table 5.2: *Statistical classes and occurrence frequencies for the 9000-sample dataset.*

The modal class is the one from 1116.60 to 1153.60 °C. The mean temperature value is 1152.50 °C, the variance is 6004.40 °C^2, and the standard deviation is 77.50 °C. Finally, the absolute statistical error is 1.60 °C, and the histogram is shown below:

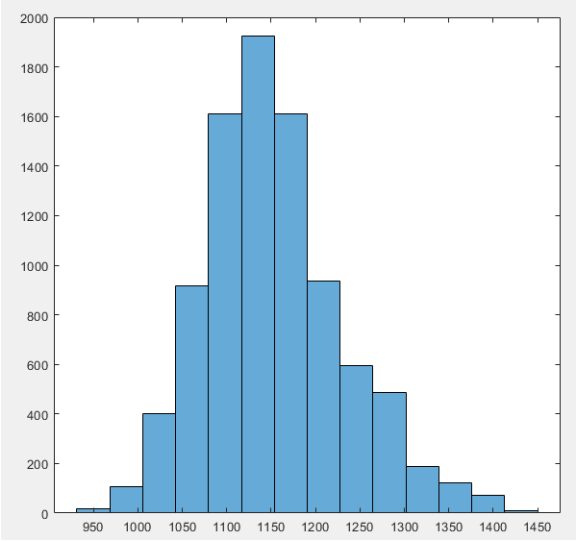

Fig 5.3: *Temperature histogram for the 9000-sample dataset.*

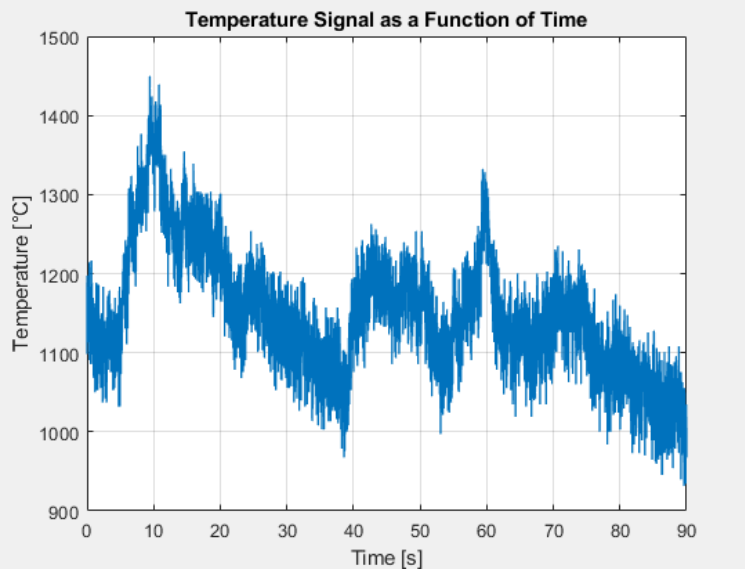

Fig 5.4: *Temperature signal as a function of time for the 9000-sample dataset.*

5.1.3 INFLUENCE OF SAMPLE SIZE ON STATISTICAL CONVERGENCE

The statistical properties obtained from the 1200-sample and 9000-sample datasets were compared in order to evaluate the influence of the acquisition length on the reliability of the temperature measurements. The table below summarizes the main statistical parameters for both datasets:

PARAMETER	**N = 1200**	**N = 9000**
NUMBER OF CLASSES	11	14
MEAN TEMPERATURE [°C]	1077.20	1152.50
VARIANCE [$°C^2$]	1535.60	6004.40
STANDARD DEVIATION [°C]	39.20	77.50
STATISTICAL ERROR [°C]	2.22	1.60

Table 5.3: *Comparison of statistical parameters for the 1200-sample and 9000-sample datasets.*

The temperature distributions corresponding to the two datasets are shown in Figures 5.1 and 5.3. The histograms provide a visual representation of the frequency distribution of the measured

temperatures and allow a direct comparison of the statistical characteristics of the two acquisitions.

The histogram corresponding to the 1200-sample dataset exhibits a relatively narrow distribution centered around a mean temperature of 1077.20 °C. The calculated standard deviation is equal to 39.20 °C, which indicates a moderate dispersion of the temperature fluctuations around the mean value. The distribution is approximately symmetric, and it seems to be a normal distribution, which suggests that the measured fluctuations are random.

The 9000-sample dataset shows a broader temperature distribution centered around a mean value of 1152.50 °C. The larger variance and standard deviation indicate a significantly wider range of temperature fluctuations with respect to the 1200-sample dataset. This is visible in the histogram, which spans a larger temperature interval when compared to the 1200-sample dataset histogram.

Even though the fluctuation amplitude is higher for the 9000-sample dataset, the statistical error is significantly lower (1.60 and 2.22 °C). This shows that the uncertainty associated with the estimate of the mean temperature decreases because of the substantially larger number of samples available for the calculation, and this is an important aspect of statistical convergence. The statistical error is proportional to the standard deviation and inversely proportional to the square root of the sample size, as shown in Equation 4.3. Consequently, increasing the acquisition length improves the confidence in the estimated mean value when the instantaneous temperature fluctuations become larger.

The comparison demonstrates the importance of acquiring large datasets when characterizing combustion temperature fields. A larger number of samples provides a better description of the temperature distribution and reduces the uncertainty associated with the mean temperature. For this reason, the 9000-sample dataset can be considered statistically more robust and reliable representation of the temperature field analyzed in this work.

5.2 SYSTEMATIC ERROR RESULTS

5.2.1 STATIC CALIBRATION AND LINEAR REGRESSION

The systematic error analysis began with the static calibration of the thermocouple. A total of 21 calibration points composed of a measured voltage and the corresponding reference temperature were available, and the following table shows the calibration dataset used for analysis:

TENSION [mV]	TEMPERATURE [°C]
0.786	400
1.791	600
2.431	700
2.784	750
3.158	800
3.551	850
3.963	900
4.395	950
4.844	1000
5.311	1050
5.793	1100
6.29	1150
6.8	1200
7.326	1250
7.866	1300
8.418	1350
8.979	1400
9.549	1450
10.124	1500
10.704	1550
11.286	1600

Table 5.4: *Calibration dataset used for thermocouple regression analysis.*

The first step was to apply the least-square linear regression, with the average voltage of 6.01 mV and the average temperature of 1088.10 °C, to the experimental data. The resulting linear calibration equation was:

$$T = 446.8304 + 106.7512V$$

Equation 5.1

Figure 5.5 shows the linear regression of the thermocouple calibration data, including the experimental calibration points.

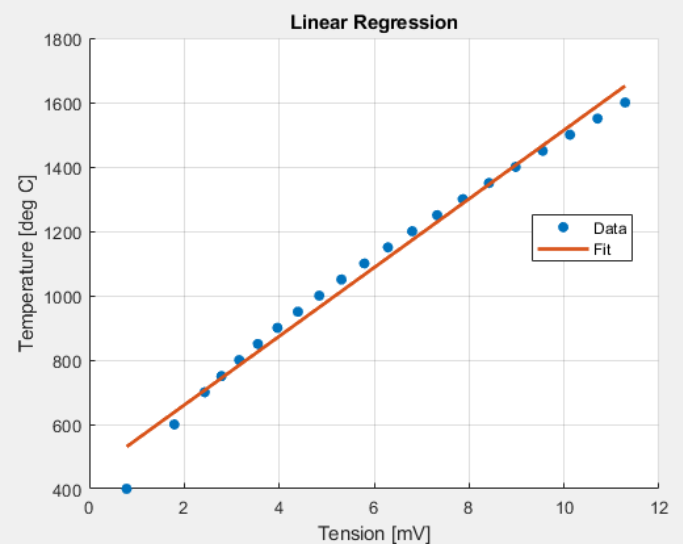

Fig 5.5: *Linear regression of thermocouple calibration data.*

The coefficient of determination obtained for the linear regression was approximately equal to 0.99. This value indicates a strong correlation between voltage and temperature. However, by analyzing Figure 5.5, it is possible to see that the thermocouple response is not perfectly linear over the entire measurement range. Small deviations are evident especially at low and high temperatures, which suggests that a higher-order interpolation may provide a more accurate representation of the calibration data.

5.2.2 COMPARISON OF POLYNOMIAL INTERPOLATION MODELS

To improve the representation of the calibration curve, polynomial regressions up to fourth order were investigated. The quality of each interpolation was evaluated using both the coefficient of determination and the standard error of regression. The following table summarizes obtained results, and Figure 5.6 shows the comparison of polynomial interpolation models, including the calibration data.

REGRESSION MODEL	R^2	STANDARD ERROR OF REGRESSION [°C]
Linear (1^{st} order)	0.9851	41.68
Quadratic (2^{nd} order)	0.9979	16.04
Cubic (3^{rd} order)	0.9997	5.81
Fourth-order	~1	2.44

Table 5.5: *Comparison of polynomial regression models.*

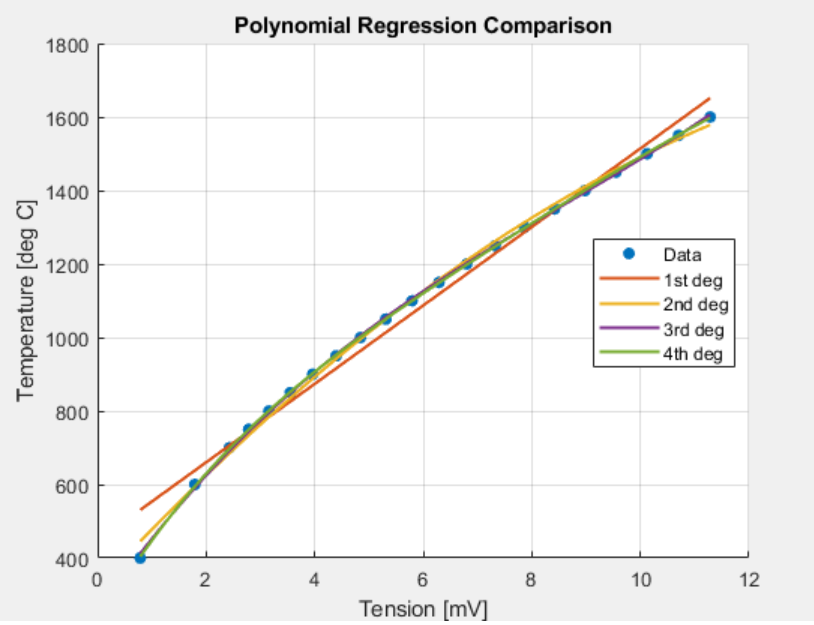

Fig 5.6: *Comparison of polynomial interpolation models for thermocouple calibration data.*

As expected, increasing the polynomial order significantly improves the agreement between the regression curve and the experimental calibration points. The coefficient of determination approaches unity, while the standard error of regression decreases substantially.

The most significant parameter for selecting the interpolation model is the standard of regression, since it quantifies the typical deviation between the calibration data and the predicted temperatures. A smaller value of σ_ε indicates that the interpolation reproduces the experimental calibration more accurately. The fourth-order polynomial produces the lowest regression standard deviation:

- $\boldsymbol{\sigma_\varepsilon = 2.54\ °C}$

which is approximately seventeen times smaller than the obtained with the linear regression model. For this reason, the fourth-order polynomial was selected as the calibration model for the systematic uncertainty analysis. Its near-perfect coefficient of determination and minimal regression error indicate that it provides the most accurate representation of the thermocouple calibration curve within the investigated temperature range.

5.2.3 EVALUATION OF THE SYSTEMATIC ERROR

The systematic error associated with the thermocouple calibration was evaluated using the regression standard deviation of the selected fourth-order polynomial and the Student`s t-distribution. For a confidence level of 95% and 19 degrees of freedom, according to the Figure 4.1, the Student coefficient is 2.09. From Equation 4.9, the systematic error of the thermocouple is:

- $\varepsilon_{sist} = 5.10\ °C$

In addition to the calibration uncertainty, the uncertainty associated with the reference instrumentation used during calibration must also be considered. According to the manufacturer`s specifications, the uncertainty of the reference instrument is equal to 0.5% of the full-scale value. Considering a full-scale temperature of 1600 degrees Celsius, the uncertainty associated with the reference instrument is:

- $\varepsilon_{instr} = 8.00\ °C$

The total systematic uncertainty is obtained by combining the two contributions, according to Equation 4.11:

- $\varepsilon_{sist,total} = 9.49\ °C$

The results show that the uncertainty associated with the reference instrumentation represents the dominant contribution to the total systematic error. Although the fourth-order polynomial interpolation reproduces the calibration data with excellent accuracy, the overall systematic uncertainty remains governed by the limitations of the calibration standard itself. This value of the total systematic error represents the bias uncertainty associated with the temperature measurements obtained using the Type-B thermocouple.

5.3 QUANTIZATION ERROR RESULTS

5.3.1 VOLTAGE SIGNAL ANALYSIS

The quantization error associated with the data acquisition system was evaluated using a time series measurement of the voltage signal generated by the type-B thermocouple. The signal was amplified by a factor of 100 before being acquired by the analog-to-digital converter (ADC). A

total of 28 voltage measurements were recorded together with their corresponding temperature values. The following table shows the voltage and temperature data used for the quantization error analysis:

TENSION [V]	TEMPERATURE [◦C]
0.795	1300.465
0.797	1302.319
0.798	1303.246
0.801	1306.027
0.801	1306.027
0.8	1305.1
0.798	1303.246
0.796	1301.392
0.796	1301.392
0.793	1298.61
0.793	1298.61
0.791	1296.756
0.793	1298.61
0.793	1298.61
0.79	1295.829
0.789	1294.902
0.786	1292.121
0.786	1292.121
0.786	1292.121
0.786	1292.121
0.787	1293.048
0.786	1292.121
0.784	1290.266
0.783	1289.339
0.78	1286.558
0.777	1283.777
0.774	1280.995
0.791	1296.756

Table 5.6: *Voltage and temperature values used for quantization error analysis.*

The average values obtained from the dataset were 0.79 V and 1296.20 °C. These values are representative of the operating conditions selected for the quantization analysis and correspond to a flame temperature close to 1300 degrees Celsius.

5.3.2 QUANTIZATION ERROR OF THE ADC

The acquisition board employed in the experimental analysis is equipped with a 12-bit-analog-to-digital converter operating over a voltage range of 0-10 V. The quantization error corresponds to half of the least significant bit (LSB) and is given by the Equation 4.12. In this case, F is 10, n is 12, and therefore the quantization error in Volts is:

- $\varepsilon_{quant,V} = 1.22 \times 10^{-3}$ V

This value represents the uncertainty introduced by the finite resolution of the ADC. However, since the quantity of interest is temperature rather than voltage, the quantization uncertainty must be converted into degrees Celsius through the error propagation. The voltage-to-temperature sensitivity was estimated using the following equation:

$$\frac{dT}{dV} = \frac{T_{max} - T_{min}}{V_{max} - V_{min}}$$

Equation 5.2

From Table 5.6, the values obtained were:

- $T_{max} = 1306.00$ °C
- $T_{min} = 1281.00$ °C
- $V_{max} = 0.80$ V
- $V_{min} = 0.77$ V

Therefore, the resulting sensitivity is:

$$\frac{dT}{dV} = 927.11 \ \frac{°C}{V}$$

The quantization error expressed in temperature units is therefore, using Equation 4.13:

- $\varepsilon_{quant} = 1.13$ °C

5.3.3 CONTRIBUTION TO THE OVERALL MEASUREMENT UNCERTAINTY

The obtained quantization uncertainty is relatively small compared to the systematic uncertainty previously evaluated for the thermocouple calibration process. The total uncertainty associated with the temperature measurement was evaluated by combining the statistical, systematic, and quantization errors, according to the following equation:

$$\varepsilon_{tot} = \sqrt{\varepsilon_{quant}^2 + \varepsilon_{stat}^2 + \varepsilon_{sist,total}^2}$$

Equation 5.3

Plugging in the values obtained in the previous sections, which are 1.13 °C, 9.49 °C, and 1.60 °C (9000-samples dataset), for the quantization, systematic, and statistical errors, respectively, the total error is:

- **ε_{tot} = 9.69 °C**

The results show that the quantization uncertainty contributes only a small fraction of the overall measurement uncertainty. The dominant contribution remains the systematic error associated with the thermocouple calibration and the reference instrumentation. Consequently, improvements in ADC resolution would produce only a limited reduction in the total uncertainty, whereas improvements in calibration accuracy would have a much greater impact on the quality of the temperature measurements.

5.4 THERMOCOUPLE RADIATION LOSSES

5.4.1 INFLUENCE OF EMISSIVITY AND GAS VELOCITY

The iterative procedure described in Chapter 4 was applied using the mean temperature value obtained from the 9000-sample dataset as the thermocouple junction temperature. The thermocouple emissivity was varied between 0.20 and 0.80, while the gas velocity was varied from 1 to 91 m/s. The objective was to quantify the influence of these parameters on the radiative losses and, consequently, on the difference between the actual gas temperature and the temperature measured by the thermocouple. The results are presented in the figure below:

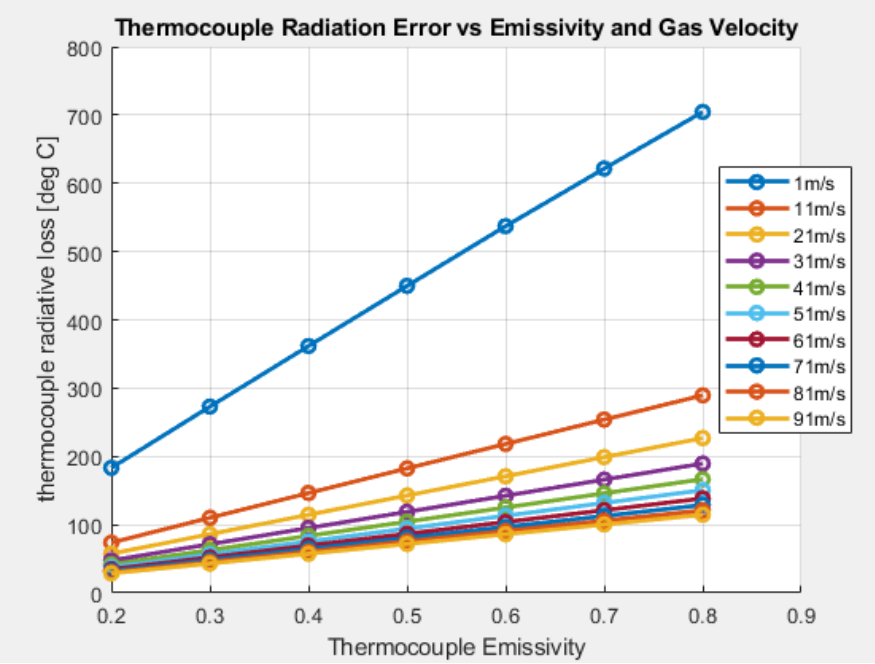

Fig 5.7: *Thermocouple radiation error vs emissivity for different gas velocities.*

Several observations can be made from this graph. First, for all gas velocities considered, the radiation loss increases approximately linearly with the thermocouple emissivity. This behavior is expected from the radiative heat transfer equation, where the radiative exchange is directly proportional to emissivity. As the thermocouple surface becomes more emissive, a larger amount of thermal radiation is emitted toward the surroundings, increasing the difference between the gas temperature and the measured junction temperature.

Second, the influence of gas velocity is very significant. At low velocities, the radiation losses become very large. For the case of a new thermocouple with emissivity equal to 0.20, and a gas velocity of only 1 m/s, the predicted radiation error is approximately 190 °C. As the emissivity increases to 0.80, the estimated error reaches values above 700 °C.

The large corrections happen because low gas velocities result in low Reynolds numbers, and therefore low convective heat transfer coefficients. Under these conditions, the thermocouple receives relatively little energy from the surrounding gas while continuing to lose energy by radiation. The junction temperature consequently becomes substantially lower than the actual gas temperature.

Increasing the gas velocity reduces the radiation error. At velocities above approximately 50 m/s, the radiation losses become considerably smaller and less sensitive to emissivity variations. For example, at 91 m/s, the correction ranges approximately from 35 °C for emissivity of 0.20 to about 115 °C for emissivity of 0.80.

This behavior is associated with the increase in convective heat transfer. As velocity increases, the Reynolds number and Nusselt number increase, resulting in a larger convective heat transfer coefficient. The thermocouple is therefore able to exchange heat efficiently with the surrounding gases, reducing the temperature difference required to balance the radiative losses.

5.4.2 IMPLICATIONS FOR TEMPERATURE MEASUREMENTS

The results demonstrate that radiation losses represent one of the most important sources of error in high-temperature thermocouple measurements. Even for relatively low emissivity values, the correction can easily exceed one hundred degrees Celsius depending on the local flow conditions.

Thermocouple aging is very relevant in this context. The exposed junction of a type-B thermocouple is continuously subject to elevated temperatures and aggressive combustion products. During operation, oxidation and surface degradation may increase the effective emissivity of the junction. As a consequence, radiation losses progressively increase with thermocouple usage, potentially introducing substantial measurement bias if no correction is applied.

The analysis also highlights the importance of accurately estimating the local gas velocity. The difference between assuming a gas velocity of 1 and 91 m/s can lead to variations of several hundred °C in the predicted correction. Therefore, reliable knowledge of the flow field is essential when radiation corrections are applied.

From an engineering perspective, these findings indicate that the temperature directly measured by the thermocouple should not be interpreted as the actual gas temperature, but it must be considered as a lower-bound estimate. The true gas temperature is expected to be higher by an amount corresponding to the radiative correction determined from the energy balance.

This is important in propulsion and gas-turbine applications, where thermal loads experienced by components such as turbine blades depend on the actual gas temperature, and not on the temperature indicated by the thermocouple. Failure to account to radiative losses may lead to a significant underestimation of the thermal environment and of the associated material and cooling requirements.

5.4.3 SELECTION OF A REALISTIC CORRECTION

The analysis was extended over a range of emissivities and gas velocities to understand the influence of these parameters on the radiative losses. However, the type-B thermocouple used in this work has a nominal emissivity close to 0.20, while the experiments were set at a flow velocity of 7 m/s.

Therefore, the final radiative loss is approximately:

- $\Delta T_{rad} = 87.50\ °C$

5.5 THERMOCOUPLE DYNAMIC ANALYSIS RESULTS

5.5.1 DYNAMIC CALIBRATION CURVE

Figure 5.8 presents the dynamic calibration signal obtained during the thermocouple response test. This sensor was subjected to a sudden temperature variation, and the transient evolution of the measured temperature was recorded.

As expected, the thermocouple does not respond instantaneously to the imposed thermal excitation. Instead, the measured temperature increases progressively from its initial value toward a final steady-state condition. The shape of the response is characteristic of a first-order thermal system, showing a rapid initial increase followed by a gradual asymptotic approach to equilibrium.

The measured temperature rises from approximately 100 °C to a final value slightly above 1000 °C. Most of the temperature increase occurs during the first 0.3 seconds, while the remaining part of the transient corresponds to the progressive stabilization of the sensor response.

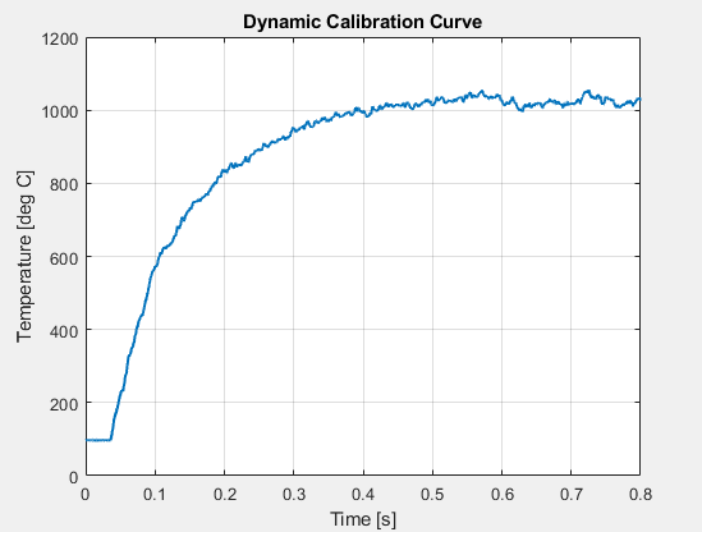

Fig 5.8: *Dynamic calibration curve of the thermocouple.*

5.5.2 FIRST-ORDER MODEL VALIDATION

The thermocouple was modeled as a first-order system according to the methodology presented in Chapter 4. Figure 5.9 compares the experimental measurements with the reconstructed first-order response obtained using the estimated time constant.

A good agreement between the experimental data and the theoretical model can be observed throughout most of the transient. Minor discrepancies are present during the early stages of the response, where the heating process is more complex and may deviate slightly from the ideal first-order thermal system.

Therefore, the overall agreement confirms that the dynamic behavior of the thermocouple can be reasonably represented by a first-order thermal system. The capability of the model to reproduce the measured response indicates that the dominant thermal mechanism governing the sensor dynamics is captured by a single time constant.

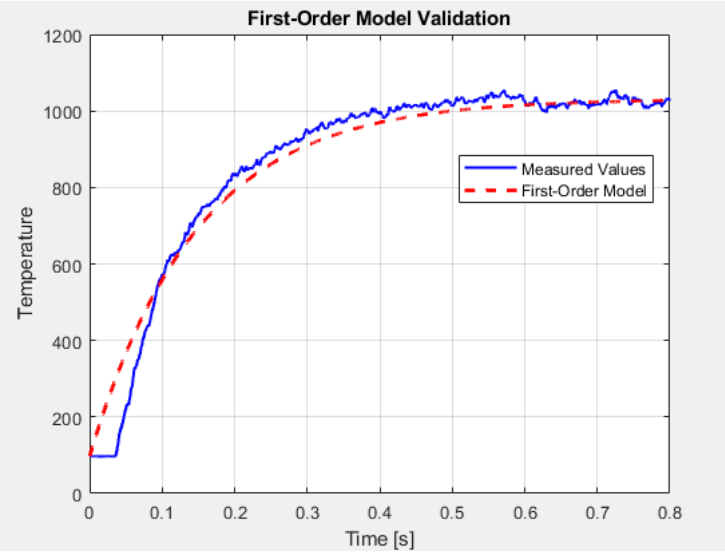

Fig 5.9: *Dynamic calibration curve: measured values vs first-order model.*

5.5.3 DIMENSIONLESS RESPONSE FUNCTION

The dimensionless response function Γ introduced in chapter 4 was evaluated from the experimental data and is shown in Figure 5.10.

The parameter Γ decreases monotonically from 1 towards zero as the thermocouple approaches thermal equilibrium. This behavior is consistent with the theoretical expression given in Equation 4.20, which characterizes the response of a first-order system. The experimental trend follows the expected exponential decay, confirming that the thermocouple exhibits the dynamic characteristics assumed in the theoretical model.

Small oscillations become visible at larger times, when Γ approaches zero. These fluctuations are mainly associated with measurement noise and have small influence on the estimation of the time constant because the fitting procedure is dominated by the initial portion of the transient.

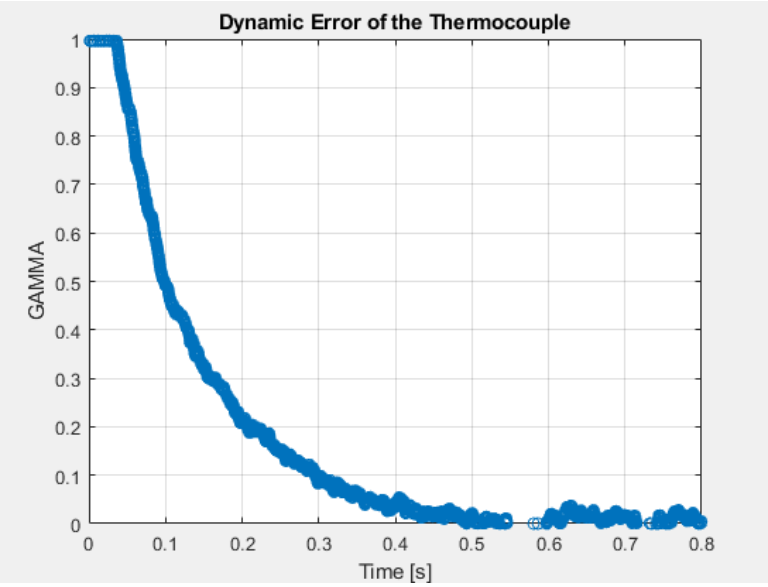

Fig 5.10: *Dynamic error of the thermocouple.*

5.5.4 DETERMINATION OF THE TIME CONSTANT

To determine the thermocouple time constant, the logarithmic transformation given by Equation 4.21 was applied to the experimental data. Figure 5.11 presents the logarithmic representation together with the least-squares linear regression. The experimental points align reasonably well with the fitted straight line, confirming the exponential nature of the thermocouple response. The slope of the regression line was obtained using the MATLAB fitting procedure described in chapter 4. From the relation given by Equation 4.22, the characteristic time constant of the thermocouple was calculated, resulting in:

- $\tau_c = 0.15$ s

This value represents the characteristic response time of the thermocouple and quantifies the rate at which the sensor reacts to a temperature change. For a first-order system, approximately 63.20% of the total temperature variation is reached after one time constant. Consequently, the thermocouple reaches 95% of the final value after approximately 0.44 seconds, and 99% of the final value after 0.74 seconds, which represents 3 time constants and 5 time constants, respectively. These values are consistent with the transient response observed experimentally in Figure 5.8.

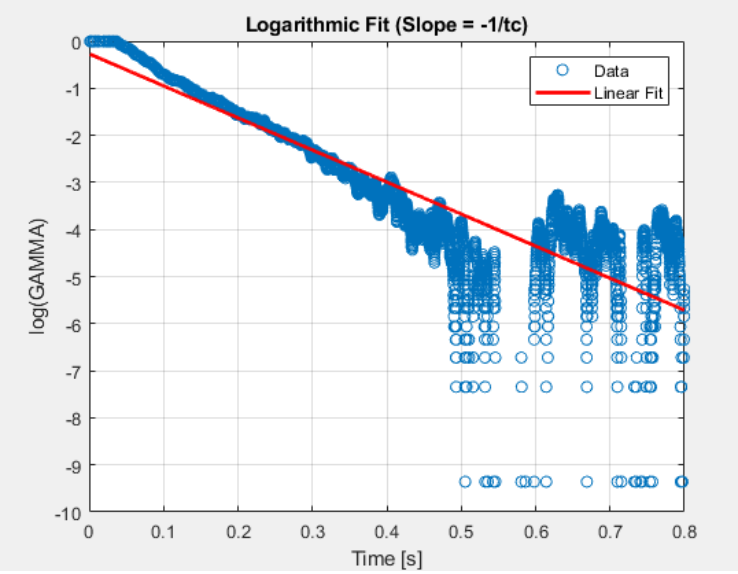

Fig 5.11: *Logarithmic representation vs linear fit*

It can be observed that the logarithmic representation deviates from the ideal linear trend for times greater than approximately 0.40 seconds. This behavior does not indicate a departure from the first-order thermocouple dynamics. As the thermocouple approaches thermal equilibrium, the dimensionless response function Γ tends toward zero and the remaining temperature difference becomes very small. Under these conditions, measurement noise, quantization effects, and small temperature fluctuations become comparable to the signal itself. The logarithmic transformation amplifies these small uncertainties, producing the scatter observed in the final portion of the curve. Consequently, the estimation of the time constant is primarily governed by the initial linear region, where the signal-to-noise ratio is significantly higher.

5.5.5 DISCUSSION OF THE DYNAMIC EFFECTS

The obtained time constant of 0.15 seconds indicates that the thermocouple has a finite but fast dynamic response for combustion measurements. However, the sensor cannot follow arbitrarily rapid temperature fluctuations.

Because the thermocouple behaves as a first-order low-pass filter, high-frequency temperature oscillations are attenuated and phase-delayed before being recorded by the acquisition system. Consequently, the measured temperature fluctuations generally underestimate the actual amplitude of the thermal oscillations present in the flame.

This phenomenon becomes important when analyzing turbulent combustion processes, where temperature fluctuations may occur over very short time scales. Local temperature peaks can therefore be higher than those indicated directly by the thermocouple measurements. This aspect is relevant in gas turbine applications, where components such as turbine blades are exposed to severe thermal loads, and their design depends strongly on the maximum temperatures experienced during operation. If the thermocouple response is not considered, rapid thermal excursions may be partially filtered by the sensor, leading to an underestimation of the actual gas temperature.

The dynamic calibration performed demonstrates that the type B thermocouple has a response that can be accurately described by a first-order model with a characteristic time constant of 0.15 seconds. This result provides a quantitative measure of the dynamic limitations of the sensor and adds an important element in the overall assessment of temperature measurement uncertainty discussed in this work.

5.6 FREQUENCY-DOMAIN ANALYSIS OF THE TEMPERATURE SIGNAL

5.6.1 EXPERIMENTAL CONDITIONS

The Fourier analysis was performed using the temperature signal acquired with the Type-B thermocouple, with a dataset consisting of 9000 samples at a sampling frequency of 100 Hz, corresponding to a total acquisition time of 90 seconds. According to the methodology described in chapter 4, the mean temperature value was first removed from the signal in order to isolate the

fluctuating component, as shown in Equation 4.23. The Fast Fourier Transform (FFT) was then applied to the fluctuating temperature signal, and the resulting one-sided spectrum was computed. The frequency resolution and Nyquist frequency were calculated according to Equations 4.28 and 4.29, respectively, and their values are:

- **$\Delta f = 0.01$ Hz**
- **$f_N = 50$ Hz**

Therefore, oscillatory phenomena with frequencies between 0 and 50 Hz could be investigated.

5.6.2 FOURIER SPECTRUM

Figure 5.12 presents the complete one-sided Fourier spectrum of the temperature signal.

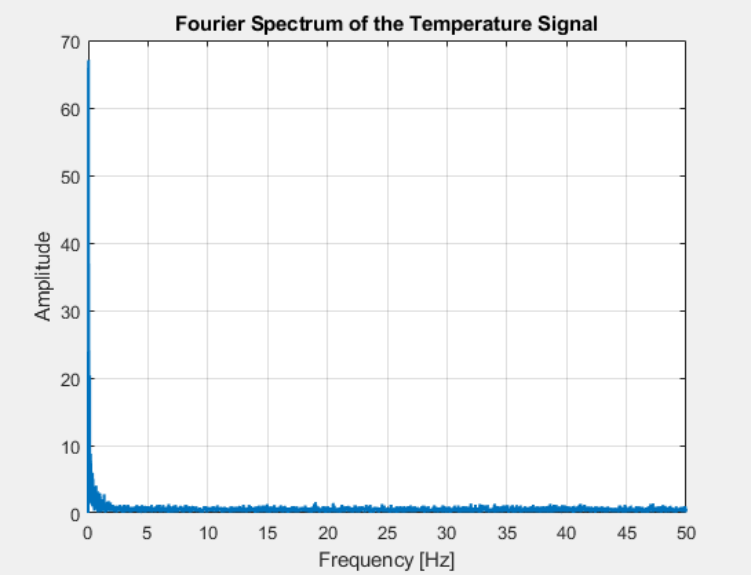

Fig 5.12: *Fourier spectrum of the temperature signal*

The spectrum is characterized by a very large concentration of energy at frequencies close to zero. The amplitude decreases rapidly as frequency increases, indicating that the temperature signal is dominated by slow thermal fluctuations.

The largest spectral amplitudes are observed below approximately 1 Hz, whereas the amplitude becomes smaller throughout the remainder of the frequency range. This behavior suggests that the thermal field generated by the burner evolves through relatively slow variations of the flame structure.

5.6.3 ZOOMED SPECTRUM AND FREQUENCY CONTENT

Because the strong low-frequency contribution masks the smaller spectral components, a second representation of the spectrum was generated using a reduced amplitude scale, as shown in Figure 5.13.

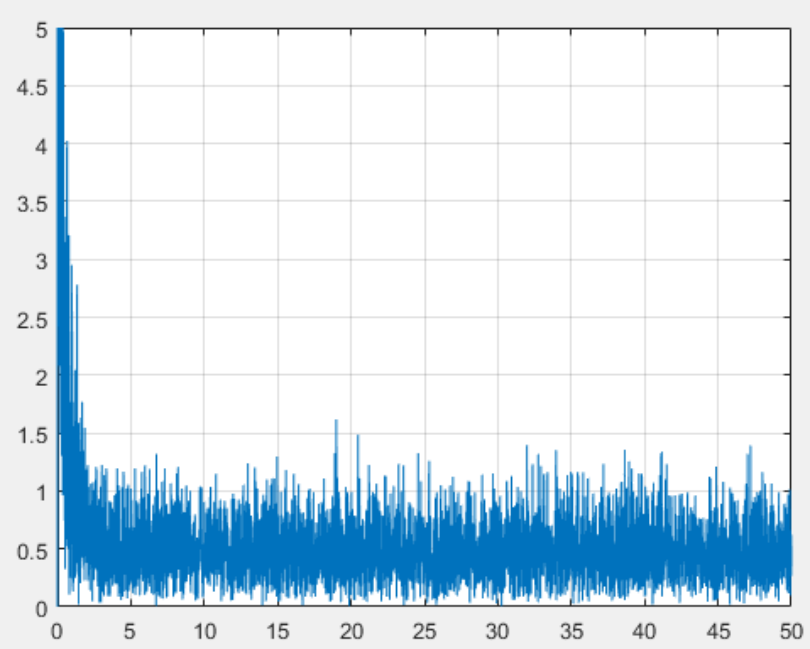

Fig 5.13: *Zoomed spectrum and frequency content*

The zoomed spectrum reveals the presence of a broadband distribution of low-amplitude fluctuations extending over the entire measurable frequency range. No distinct narrow peaks are observed. The spectral energy appears distributed over a wide range of frequencies with amplitudes below approximately 1 to 1.50 °C.

The absence of dominant peaks indicates that the combustion process did not exhibit significant periodic oscillations. There is no evidence of organized periodic phenomena, such as resonant combustion modes or thermoacoustic instabilities. These phenomena are characterized by sharp peaks at specific frequencies that correspond to oscillations modes of the burner-flame system.

5.6.4 INFLUENCE OF THERMOCOUPLE DYNAMICS

The results of the Fourier analysis must be interpreted together with the dynamic characterization presented in Section 5.5. The thermocouple time constant obtained from the dynamic calibration was 0.15 seconds. For a first-order system, the corresponding cutoff frequency is approximately:

$$f_c = \frac{1}{2\pi\tau}$$

Equation 5.4

- **f_c = 1.08 Hz**

This value represents the frequency above which the thermocouple progressively attenuates the amplitude of temperature fluctuations. Consequently, fluctuations occurring at frequencies significantly higher than approximately 1 Hz are increasingly filtered by the thermal inertia of the sensor. The measured spectrum therefore represents not only the actual frequency content of the flame but also the filtering effect introduced by the thermocouple.

The strong concentration of energy at low frequencies observed in Figures 5.12 and 5.13 is therefore consistent with the dynamic behavior identified during the calibration procedure.

5.6.5 DISCUSSION OF THE COMBUSTION PROCESS

The spectral analysis indicates that the combustion process was characterized mainly by low-frequency and stochastic temperature fluctuations. The broadband nature of the spectrum suggests that the observed fluctuations originate from turbulent mixing processes, flame front motion, and local variations in the heat release rate.

The absence of significant spectral peaks is a positive result because it indicates stable combustion. Periodic oscillations associated with combustion instabilities can produce large pressure and temperature fluctuations that may increase thermal stress, vibrations, and component fatigue in combustion systems.

The Fourier analysis therefore confirms that the investigated burner operated under stable conditions and that the measured temperature fluctuations were primarily associated with normal turbulent combustion phenomena.

5.7 FINAL TEMPERATURE EVALUATION AND OVERALL MEASUREMENT UNCERTAINTY

The objective of the analyses presented in this chapter was to quantify the different sources of error affecting the temperature measurements performed with the Type-B thermocouple and to determine the most reliable estimate of the actual gas temperature within the combustion chamber. The statistical uncertainty, systematic uncertainty, quantization error, thermocouple radiation losses, dynamic response, and frequency-domain characteristics of the measured signal were evaluated separately in order to understand their respective contributions to the final measurement quality.

The mean temperature obtained from the 9000-sample dataset was:

- $\mathbf{T_{measured} = 1152.50\ °C}$

This value corresponds to the average temperature indicated by the thermocouple hot junction and therefore represents the sensor temperature rather than the actual gas temperature. Consequently, several corrections and uncertainty contributions must be considered before estimating the true temperature of the combustion gases.

5.7.1 SUMMARY OF UNCERTAINTY SOURCES

The statistical analysis presented in section 5.1 resulted in a statistical uncertainty equal to:

- $\mathbf{\varepsilon_{stat} = \pm 1.60\ °C}$

The systematic uncertainty associated with the thermocouple calibration procedure and interpolation model was determined in section 5.2 as:

- $\mathbf{\varepsilon_{syst} = \pm 9.49\ °C}$

The quantization uncertainty introduced by the analog-to-digital conversion process was evaluated in section 5.3 and resulted in:

- $\mathbf{\varepsilon_{quant} = \pm 1.13\ °C}$

Assuming independence between the different uncertainty sources, the total uncertainty was calculated using Equation 5.3, which resulted in:

- $\varepsilon_{tot} = \pm 9.69\ °C$

The results are summarized in the table below:

SOURCES OF UNCERTAINTY	VALUE [DEGREES CELSIUS]
Statistical Error	±1.60
Systematic Error	±9.49
Quantization Error	±1.13
Total Uncertainty	±9.69

Table 5.7: *Summary of the uncertainty sources.*

Table 5.7 shows that the systematic error is the dominant contributor to the overall uncertainty. The statistical and quantization uncertainties are relatively small, indicating that the acquisition system and the sample size adopted for the measurements provide satisfactory measurement precision.

5.7.2 RADIATION CORRECTION AND GAS TEMPERATURE ESTIMATION

Although the uncertainty analysis quantifies the confidence interval associated with the measurements, the thermocouple reading must still be corrected for radiation losses.

As discussed in section 5.4, the thermocouple continuously exchanges thermal radiation with the colder surroundings. As a consequence, part of the heat received from the combustion gases is lost through radiation, causing the thermocouple temperature to be lower than the actual gas temperature.

The radiation correction depends primarily on thermocouple emissivity, gas velocity, junction temperature, and surrounding temperature. A study was performed considering thermocouple emissivities ranging from 0.20 to 0.80 and gas velocities ranging from 1 to 100 m/s. The results demonstrated that the radiation correction increases significantly as emissivity increases, since larger emissivities produce stronger radiative heat losses. The gas velocity also influences significantly the radiative heat losses, and the results showed that increasing the gas velocity

enhances convective heat transfer between the gas and the thermocouple junction, reducing the temperature difference between the measured temperature and the actual gas temperature.

For the nominal emissivity value of 0.20, representative of a clean Type-B thermocouple junction, the radiation correction remained relatively small compared with the measured temperature. However, for aged thermocouples characterized by higher emissivities, the correction became considerably larger. The corrected gas temperature is obtained from:

$$T_{\text{gas}} = T_{\text{measured}} + \Delta T_{\text{rad}}$$

Equation 5.5

where ΔT_{rad} represents the radiation correction obtained from the iterative procedure described in section 5.4. Considering the nominal emissivity of 0.20 and a nominal gas velocity of 7 m/s, which is characteristic of this kind of burner, the radiation correction is:

- **ΔT_{rad} = 87.50 °C**

The final estimated gas temperature is therefore:

- **T_{gas} = 1240 °C**

and the following figure shows the gas temperature (including the radiation correction) and the uncertainty, where the uncertainty interval accounts for the statistical, systematic, and quantization uncertainties of the measurements system.

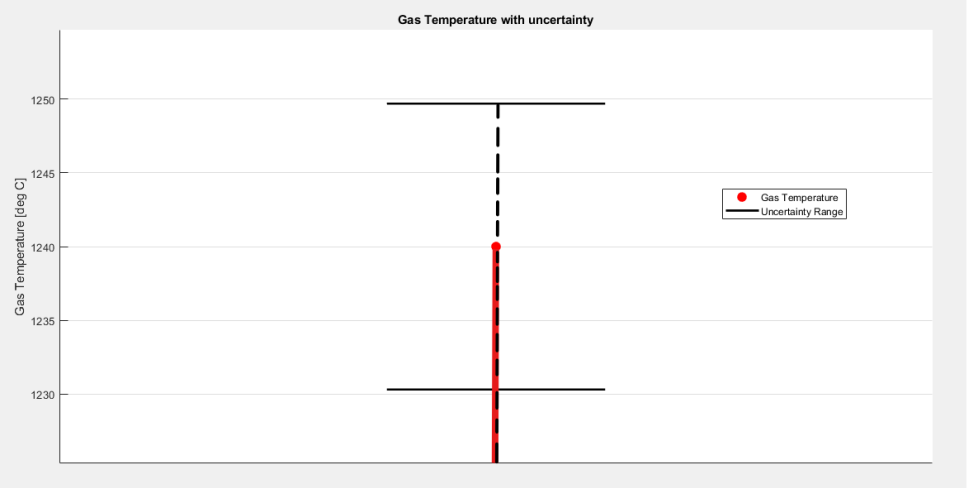

Fig 5.14: *Final gas temperature with uncertainty bounds.*

5.7.3 DYNAMIC RESPONSE ASSESSMENT

The dynamic calibration performed in section 5.5 showed that the thermocouple can be accurately represented as a first-order system. The estimated thermocouple time constant was:

- $\tau_c = 0.15$ s

This value represents the characteristic response time of the sensor and indicates the speed with which the thermocouple reacts to sudden temperature changes. For a first-order system, approximately 99% of the final value is reached after a time interval equal to five time constants:

- $t_{99} = 5\tau_c = 0.73$ s

Consequently, thermal phenomena occurring on significantly shorter time scales may be partially attenuated by the thermocouple thermal inertia. It is important to note that the dynamic analysis does not introduce a correction to the measured mean temperature. Instead, it provides information regarding the capability of the sensor to follow rapid temperature fluctuations and therefore represents a characterization of the measurement system rather than a source of measurement bias.

5.7.4 FREQUENCY-DOMAIN ANALYSIS

The Fourier analysis presented in section 5.6 provided additional information regarding the temporal characteristics of the measured temperature signal. The acquisition parameters, such as sampling frequency, number of samples, frequency resolution, and Nyquist frequency are, respectively:

- $f_s = 0.15$ s
- $N = 9000$
- $\Delta f = 0.01$ Hz
- $f_N = 50$ Hz

The obtained spectra revealed that most of the fluctuating energy was concentrated at low frequencies, while the amplitude of the high-frequency components progressively decreased.

No large peaks associated with strong combustion instabilities were observed within the measurable frequency ranges. Instead, the spectra showed predominantly broadband behavior, which is characteristic of turbulent combustion processes and random flame fluctuations.

The Fourier analysis therefore confirms that the measured temperature fluctuations are mainly governed by stochastic turbulent phenomena rather than by periodic oscillatory mechanisms.

5.7.5 FINAL REMARKS

The analyses performed throughout this chapter provide a characterization of the thermocouple measurement system and establish the confidence level associated with the experimental temperature measurements. The results indicate that:

- The statistical uncertainty is small due to the large number of samples acquired.
- The quantization error introduced by the acquisition system is negligible compared with the calibration uncertainty.
- The systematic error associated with thermocouple calibration is the dominant contributor to the overall uncertainty.
- Radiation losses produce a measurement bias and must be considered when estimating the actual gas temperature.
- The thermocouple has a characteristic time constant of 0.15 seconds, which limits its ability to resolve extremely fast thermal transients.
- The temperature fluctuations are predominantly low-frequency and broadband in nature, consistent with turbulent combustion phenomena.

Overall, the experimental methodology adopted in this work provides reliable temperature measurements with a total uncertainty of 9.69 degrees Celsius. After accounting for radiation losses, the resulting gas temperature estimate constitutes the most accurate representation of the thermal field that can be obtained with the present measurement system.

CHAPTER 6

CONCLUSIONS

This thesis investigated the accuracy of hot-gas temperature measurements performed using a Type-B thermocouple in a premixed methane-air combustion system. Attention was given to the identification, quantification, and correction of the many sources or errors affecting thermocouple measurements, including statistical uncertainty, systematic calibration errors, quantization effects, radiative heat losses, and dynamic response limitations. The final goal was to determine a more representative estimate of the actual gas temperature and to evaluate the reliability of thermocouple measurements in high-temperature combustion environments.

The experimental investigation was carried out using a 10 kW premixed methane-air burner representative of domestic combustion applications. Temperature measurements were acquired through a dedicated data-acquisition system and then analyzed using statistical, calibration, dynamic, and spectral techniques.

The statistical analysis demonstrated the importance of acquiring a sufficiently large number of samples in order to obtain reliable temperature estimates. The comparison between datasets containing 1200 and 9000 samples showed that increasing the sample size reduced the statistical uncertainty and improved the stability of the calculated mean temperature. For the selected dataset of 9000 samples, the statistical error was limited to approximately 1.60 degrees Celsius, confirming that random fluctuations associated with sampling represented only a minor contribution to the overall uncertainty.

The systematic uncertainty associated with the thermocouple calibration procedure was evaluated through static calibration experiments. Several interpolation models were compared,

including linear and higher-order polynomial regressions. The fourth-order polynomial provided the lowest interpolation standard deviation and was therefore selected as the calibration model. The resulting total systematic error was estimated to be approximately 9.50 degrees Celsius, representing one of the most significant contributors to the overall measurement uncertainty.

The analysis of the acquisition system showed that quantization effects introduced by the 12-bit analog-to-digital converter were relatively small. Through error propagation, the quantization uncertainty was estimated to be approximately 1.13 degrees Celsius. Although not negligible, this contribution was considerably smaller than the systematic calibration uncertainty.

One of the most important error mechanisms in high-temperature measurements is the thermocouple radiation losses. The analysis demonstrated that the magnitude of the correction is strongly dependent on both thermocouple emissivity and gas velocity. Higher emissivities increase radiative heat losses and consequently increase the difference between the measured junction temperature and the actual gas temperature, while higher gas velocities enhance convective heat transfer and reduce the magnitude of the correction. The results confirmed that the measured temperature can significantly underestimate the true gas temperature if radiation losses are neglected.

The dynamic calibration of the thermocouple showed that the sensor behaves approximately as a first-order system characterized by a time constant of 0.15 seconds. This result indicates that the thermocouple is capable of accurately tracking relatively slow temperature variations but may attenuate rapid thermal fluctuations occurring at frequencies higher than its characteristic response frequency. Consequently, measured temperature peaks may be lower than the actual instantaneous gas temperatures.

The Fourier analysis provided additional information into the temporal characteristics of the temperature signal. The frequency spectrum revealed that most of the fluctuation energy was concentrated at low frequencies, while no significant high-frequency combustion instabilities were detected within the measurable frequency range. This observation is consistent with the dynamic analysis and suggests that the thermocouple was able to capture the dominant thermal fluctuations occurring within the flame.

By combining the different uncertainty contributions, the overall measurement uncertainty was estimated to be approximately 9.69 degrees Celsius. The measured mean temperature obtained during the experiments was 1152.50 degrees Celsius. When combined with the uncertainty analysis and radiation losses, which were approximately 87.50 degrees Celsius, this value provides a more realistic estimate of the actual thermal conditions present within the combustion chamber. Therefore, the final estimate considered was 1240 degrees Celsius with uncertainty of ±9.69 degrees Celsius.

From an engineering perspective, the results highlight the importance of thermocouple measurements before using them for combustion analysis or component design. Gas turbine combustors, combustion chambers, turbine blades and other components operate under severe thermal conditions, and design decisions based solely on raw thermocouple readings may lead to an underestimation of the actual loads experienced by the components. Therefore, the radiation loss and the upper bound of the uncertainty must be added to the mean temperature registered by the thermocouple. The methodology developed in this work therefore provides a practical framework for improving the reliability of high-temperature measurements and obtaining more representative gas temperature estimates.

Future developments of this work could include the extension of the measurements to multiple radial and axial locations in order to reconstruct complete temperature fields within the flame. Future work could also include extending the methodology to more realistic gas turbine conditions, such as tests in aviation combustors and the use of practical aviation fuels such as kerosene, in order to assess the influence of spray combustion, increased radiation levels, and more complex flow structures on thermocouple measurement accuracy. Furthermore, the experimental results could be compared with numerical simulations in order to validate combustion and heat-transfer models and further improve the accuracy of temperature predictions.

BIBLIOGRAPHY

[1] M.V. Mekhrengin, I.K. Meshkovskii, V.A. Tashkinov, V.I. Guryev, A.V. Sukhinets, and D.S. Smirnov. “Multispectral pyrometer for high temperature measurements inside combustion chamber of gas turbine engines”. *Measurement*, 139:355–360, 2019.

[2] F. Rinaldi, B. Najafi. “Temperature Measurement in WTE Boilers Using Suction Pyrometers”. *Sensors*, 13(11):15633-15655, 2013.

[3] D. L. Elmore, W. W. Robinson, and W. B. Watkins. “Dynamic Gas Temperature Measurement System Final Report”. *NASA*, *Technical Efforts*, 1, CR-168267, 1983.

[4] ThermocoupleInfo. “Thermocouple Information and Reference Tables”. *ThermocoupleInfo.com*

[5] G. W. Burns, M. G. Scroger, G. F. Strouse, M. C. Croarkin, and W. F. Guthrie. “Temperature-Electromotive Force Reference Functions and Tables for the Letter-Designated Thermocouple Types Based on the ITS-90”. *NIST Monograph*, 175, 1993.

[6] G. Solero. “Sperimentazione nei Propulsori Aeronautici – Lezione 8, Parte Prima”. *M.Sc. Course in Aeronautical Engineering, Politecnico di Milano*, 2025. Unpublished lecture notes.

[7] N. Yilmaz, W. Gill, A.B. Donaldson, and R.E. Lucero. “Problems Encountered in Fluctuating Flame Temperature Measurements by Thermocouple”. *Sensors*, 8(12):7882–7893, 2008.

[8] Sphaera Training Systems. “Engine Temperature Indicator (EGT gauge) CBT”. *Sphaera Training Systems*. https://sphaera.co.uk/

[9] Royal Air Force (RAF). “AP3456: The Central Flying School (CFS) Manual of Flying, Volume 5 – Flight Instruments”. *The Central Flying School, United Kingdom*.

[10] W. L. Tew, and G. F. Strouse. “Standard Reference Material 1750: Standard Platinum Resistance Thermometers, 13.8033 K to 429.7485 K”. *NIST Special Publication 260-139*, National Institute of Standards and Technology, 2001.

[11] J.V. Pearce, R. L. Rusby, K. Yamazawa, S. Rudtsch, L. Iacomini, G. Lopardo, D. R. White, and W. L. Tew. “Guide on Secondary Thermometry: Industrial Platinum Resistance Thermometers”. *International Bureau of Weights and Measures*, 2022.

[12] ILX Lightwave Corportation. “Callendar-Van Dusen Equation and RTD Temperature Sensors”. *TECH NOTE*, *TN-RTD1.*

[13] National Institute of Standards and Technology (NIST). “Mercury Thermometer Alternatives: Platinum Resistance Thermometers (PRTs)”. NIST, 2011.

[14] A. Ward. “PT100 platinum resistance thermometers”. *Pico Technology*, 2025. https://www.picotech.com

[15] M. Petkovšek, M. Nemec, and P. Zajec. “Algorithm Execution Time and Accuracy of NTC Thermistor-Based Temperature Measurements in Time-Critical Applications”. *Mathematics*, 9(18), 2021.

[16] M. Schubert, C. Münch, S. Schuurman, V. Poulain, J. Kita, and R. Moos. “Thermal Treatment of Aerosol Deposited $NiMn_2O_4$ NTC Thermistors for Improved Aging Stability”. *Sensors*, 18(11), 2018.

[17] C. -C. Wang, Z. -Y. Hou, and J. -C. You. “A High-Precision CMOS Temperature Sensor with Thermistor Linear Calibration in the (−5 °C, 120 °C) Temperature Range”. *Sensors*, 18(7), 2018.

[18] EEEGUIDE.COM. “Thermistor Operation”. *EEEGUIDE.COM – Online Electrical and Electronics Learning Site.* https://www.eeeguide.com

[19] Textron Aviation. “300-0656-2 Thermistor Assembly”. *Textron Aviation Parts Catalog. https://ww2.txtav.com*

[20] Y. Huang, J. Long, D. Chen, M. Long, Z. Yang, and C. Li. “Temperature Errors in Two-Color Pyrometry Simultaneously Considering Reflection and Combustion Gas Radiation”. *Optics Express*, 29(16):25084-25099, 2021.

[21] N. Docquier, and S. Candel. “Combustion Control and Sensors: A Review”. *Progress in Energy and Combustion Science*, 28(2):107-150, 2002.

[22] Britannica Editors. “Planck’s radiation law”. *Encyclopedia Britannica*, 2025. https://www.britannica.com/science/Plancks-radiation-law

[23] G. Solero. “Sperimentazione nei Propulsori Aeronautici – Lezione 8, Parte Seconda”. *M.Sc. Course in Aeronautical Engineering, Politecnico di Milano*, 2025. Unpublished lecture notes.

[24] R. Nave. “Spectral Colors”. *HyperPhysics, Georgia State University*. http://hyperphysics.phy-astr.gsu.edu/hbase/vision/specol.html

[25] D. Li, C. Feng, S. Gao, K. Daniel, and L. Chen. “Effect of Pyrometer Type and Wavelength Selection on Temperature Measurement Errors for Turbine Blades”. *Infrared Physics & Technology*, 94:255-262, 2018.

[26] R. Usamentiaga, P. Venegas, J. Guerediaga, L. Vega, J. Molleda, and F. G. Bulnes. “Infrared Thermography for Temperature Measurement and Non-Destructive Testing”. *Sensors*, 14(7):12305-12348, 2014.

[27] S. Bagavathiappan, B.B. Lahiri, T. Saravanan, J. Philip, and T. Jayakumar. “Infrared Thermography for Condition Monitoring – A Review”. *Infrared Physics & Technology*, 60:35-55, 2013.

[28] F. Li, J. Pan, C. Zhang, E. K. Quaye, and X. Shao. “Structure and Combustion Characteristics of Methane/Air Premixed Flame under the Action of Wall.” *Energy Engineering*, 118(4):1135–1154, 2021.

[29] NASA Glenn Research Center. “The Process of Combustion”. *National Aeronautics and Space Administration (NASA).* https://www.grc.nasa.gov

[30] G. Bagheri, E. Ranzi, M. Pelucchi, A. Parente, A. Frasoldati, and T. Faravelli. “Comprehensive Kinetic Study of Combustion Technologies for Low Environmental Impact: MILD and OXY-fuel Combustion of Methane”. *Combustion and Flame*, 212:142-155, 2020.

[31] C. Paravan. “Combustion in Thermochemical Propulsion – Chapter 1”. *M.Sc. Course in Aeronautical Engineering, Politecnico di Milano*, 2024. Unpublished lecture notes.

[32] C. Paravan. “Combustion in Thermochemical Propulsion – Chapter 2, Part 1”. *M.Sc. Course in Aeronautical Engineering, Politecnico di Milano*, 2024. Unpublished lecture notes.

[33] A. Sakhrieh. “The Adiabatic Flame Temperature and Laminar Flame Speed of Methane Premixed Flames at Varying Pressures”. *Acta Periodica Technologica*, 220-227, 2019.

[34] O. Labban. “Introduction to EES – 2. Fundamentals of Advanced Energy Conversion”. *Massachusetts Institute of Technology*, 2018. Unpublished lecture notes.

[35] N. Yilmaz, W. Gill, A. B. Donaldson, and R. E. Lucero. “Problems Encountered in Fluctuating Flame Temperature Measurements by Thermocouple”. *Sensors*, 8(12):7882-7893, 2008.

[36] L. A. Moreno-Pacheco, F. Sanchez-Lopez, J. G. Barbosa-Saldana, J. Martinez-Trinidad, M. A. Carpinteyro-Perez, W. Wong-Angel, and R. A. Garcia-Leon. “Design and Numerical Analysis of an Annular Combustion Chamber”. *Fluids*, 9(7), 161, 2024.

[37] G. Solero. “Sperimentazione nei Propulsori Aeronautici – Lezione Zero”. *M.Sc. Course in Aeronautical Engineering, Politecnico di Milano*, 2025. Unpublished lecture notes.

[38] C. Paravan. “Combustion in Thermochemical Propulsion – Chapter 8, Part 1”. *M.Sc. Course in Aeronautical Engineering, Politecnico di Milano*, 2024. Unpublished lecture notes.

[39] R. Harkins. “Sturge`s Rule: A Method for Selecting the Number of Bins in a Histogram”. *The Manufacturing Academy*. https://accendoreliability.com

[40] G. Solero. “Sperimentazione nei Propulsori Aeronautici – Lezione 1, Parte Prima”. *M.Sc. Course in Aeronautical Engineering, Politecnico di Milano*, 2025. Unpublished lecture notes.

[41] G. Solero. “Sperimentazione nei Propulsori Aeronautici – Lezione 1, Parte Seconda”. *M.Sc. Course in Aeronautical Engineering, Politecnico di Milano*, 2025. Unpublished lecture notes.

[42] G. Solero. “Sperimentazione nei Propulsori Aeronautici – Lezione 2, Parte Prima”. *M.Sc. Course in Aeronautical Engineering, Politecnico di Milano*, 2025. Unpublished lecture notes.

[43] D. C. Montgomery, E. A. Peck, and G. G. Vining. “Introduction to Linear Regression Analysis (5th ed)”. John Wiley & Sons.

[44] G. Solero. “Sperimentazione nei Propulsori Aeronautici – Lezione 3”. *M.Sc. Course in Aeronautical Engineering, Politecnico di Milano*, 2025. Unpublished lecture notes.

[45] G. Solero. “Sperimentazione nei Propulsori Aeronautici – Lezione 9”. *M.Sc. Course in Aeronautical Engineering, Politecnico di Milano*, 2025. Unpublished lecture notes.

[46] S. W. Churchill, and M. Bernstein. “A Correlating Equation for Forced Convection From Gases and Liquids to a Circular Cylinder in Crossflow”. *Journal of Heat Transfer*, 99(2), 300-306, 1977.

[47] G. Solero. “Sperimentazione nei Propulsori Aeronautici – Lezione 4”. *M.Sc. Course in Aeronautical Engineering, Politecnico di Milano*, 2025. Unpublished lecture notes.

[48] A. V. Oppenheim, R. W. Schafer, and J. R. Buck. “Discrete-Time Signal Processing (Second Edition)”. *Upper Saddle River, NJ: Prentice Hall*, 1999.

[49] J. S. Bendat, and A. G. Piersol. “Random Data: Analysis and Measurement Procedures”. John Wiley & Sons.

[50] E. O. Brigham. “The Fast Fourier Transform (FFT) and its Applications”. *Prentice-Hall*, 1988

[51] G. F. Strouse. “Standard Platinum Resistance Thermometer Calibrations from the Ar TP to the Ag FP”. *NIST Special Publication 250-81*, National Institute of Standards and Technology, 2013.

[52] T.K. Rusch. “Understanding Radiation Thermometry – Part I”. *NASA Stennis Space Center*, *NASA Technical Reports Server*, 1995.
https://ntrs.nasa.gov/api/citations/20150021314/downloads/20150021314.pdf

[53] R. B. Hathaway, and K. W. Long. “Transducers and Data Acquisition.” In Y. -L. Lee, J. Pan, R. B. Hathaway, and M. E. Barkey, “Fatigue Testing and Analysis: Theory and Practice”, 1-56. *Elsevier*, 2005.

[54] B. J. McBride, and S. Gordon. “Computer Program for Calculation of Complex Chemical Equilibrium Compositions and Applications. Part 1: Analysis”. *NASA Reference Publication 1311*, 1994.